

Manuscript version: Author's Accepted Manuscript

The version presented in WRAP is the author's accepted manuscript and may differ from the published version or Version of Record.

Persistent WRAP URL:

<http://wrap.warwick.ac.uk/145730>

How to cite:

Please refer to published version for the most recent bibliographic citation information. If a published version is known of, the repository item page linked to above, will contain details on accessing it.

Copyright and reuse:

The Warwick Research Archive Portal (WRAP) makes this work by researchers of the University of Warwick available open access under the following conditions.

© 2020 Elsevier. Licensed under the Creative Commons Attribution-NonCommercial-NoDerivatives 4.0 International <http://creativecommons.org/licenses/by-nc-nd/4.0/>.



Publisher's statement:

Please refer to the repository item page, publisher's statement section, for further information.

For more information, please contact the WRAP Team at: wrap@warwick.ac.uk.

A review of current collectors for Lithium-ion batteries

Pengcheng Zhu^a, Dominika Gastol^b, Jean Marshall^a, Roberto Sommerville^b,
Vannessa Goodship^a, Emma Kendrick^{b, *}

^aWMG, University of Warwick, Coventry, CV4 7AL, United Kingdom

^bSchool of Metallurgy and Materials, University of Birmingham, Edgbaston, Birmingham B15
2TT, United Kingdom

*Corresponding author

E.Kendrick@bham.ac.uk (Professor Emma Kendrick)

Highlights:

- Six different types of current collector materials for batteries are reviewed and compared for performance, stability, cost and sustainability.
- 2D and 3D structures of foil, mesh and foam and 2D foil surface treatments; chemical etching and coating, are discussed
- The future direction and opportunities for 2D and 3D current collectors in battery applications are provided

24 **Abstract**

25 Lithium-ion batteries are the state-of-the-art power source for most consumer
26 electronic devices. Current collectors are indispensable components bridging lithium-
27 ion batteries and external circuits, greatly influencing the capacity, rate capability and
28 long-term stability of lithium-ion batteries. Conventional current collectors, Al and Cu
29 foils have been used since the first commercial lithium-ion battery, and over the past
30 two decades, the thickness of these current collectors has decreased in order to
31 increase the energy density. However to improve the performance further, alternative
32 materials and structures, as well as specific treatments such as etching and carbon
33 coating, have also been investigated to enhance the electrochemical stability and
34 electrical conductivity of current collectors, for next-generation lithium-ion batteries
35 with higher capacities and longer service lifetime. This work reviews six types of
36 materials for current collectors, including Al, Cu, Ni, Ti, stainless steel and
37 carbonaceous materials, and compares these materials from five aspects of
38 electrochemical stability, electrical conductivity, mechanical property, density and
39 sustainability. The effects of three different structures of foil, mesh and foam as well
40 as two treatments of chemical etching and coating are also discussed. Future
41 opportunities are highlighted at the end of this review.

42

43 Keywords: Current collector, lithium-ion battery, metal, carbonaceous material

44

45 **1. Introduction**

46 The Lithium-ion battery (LIB) is currently the most commercially successful power
47 storage and generation device due to its comprehensive superiority in power density,
48 energy density, cost and safety [1]. LIBs store electricity in chemicals and convert
49 chemical energy into electricity via electrochemical reactions, which have been
50 regarded as a clean source of energy [2]. Their high energy and power densities
51 enable LIBs to power not only portable devices, e.g. phones, tablets and laptops, but
52 also electric vehicles, effectively reducing the consumption of fossil fuels and
53 greenhouse gas emission [3-5]. Furthermore, the high energy conversion rate of LIBs
54 enables them to be employed in electrical grid applications, allowing efficient storage
55 of energy harvested from renewable sources, e.g. wind, solar and geothermal [6]. It is
56 predicted that LIBs will continue to play an omnipresent role in our daily life.

57 A typical LIB is composed of a cathode, an anode, a separator, electrolyte and two
58 current collectors, as shown in Fig. 1a. Commonly used cathodes include LiCoO_2 ,
59 (LCO) LiMn_2O_4 (LMO), LiFePO_4 (LFP), and LiNiMnCoO_2 (NMC) and the anode mainly
60 used is graphite [7, 8], which more recently contains additional active components
61 such as SiO_x to improve the capacity [9]. During discharging, Li-ions stored at the
62 anode move to the cathode, generating electrons and forming current flow. The
63 process is reversed when the battery is being charged. Electrolytes consist of lithium
64 salts, e.g. LiPF_6 , LiBF_4 , LiClO_4 , in some organic solvents, e.g. propylene carbonate
65 (PC), ethylene carbonate (EC), ethyl methyl carbonate (EMC), dimethyl carbonate
66 (DMC), diethyl carbonate (DEC), that act as the conductive pathway for Li-ions
67 movement [10]. Separators, normally microporous layers consisting of either
68 polymeric membranes or non-woven fabric mats, are placed between the cathode and
69 anode to prevent physical contact [11]. Current collectors are bridging components
70 that collect electrical current generated at the electrodes and connect with external
71 circuits. Commercial current collectors are Al and Cu foils for cathodes and anodes,
72 respectively [12].

73 In 1998, Johnson and White systematically characterised some commercial LIBs
74 produced by five dominant manufacturers [13], including Sony, Moli Energy, A & T
75 Battery, Sanyo Electric and Matsushita Electric Industrial. Taking the average value
76 from the five manufacturers, the weight percentages of cathode, anode, Al foil, Cu foil,

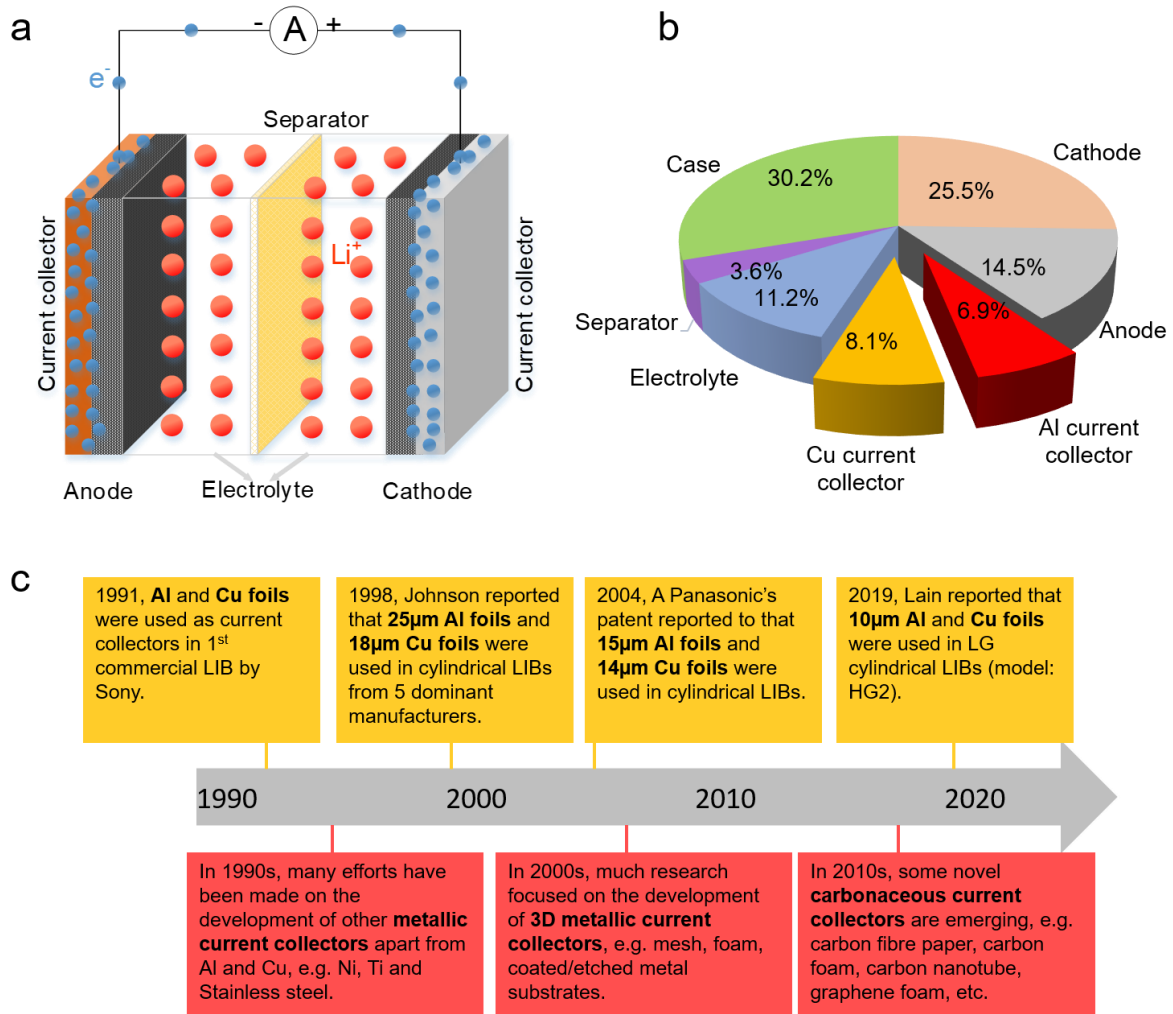
77 separator and other components are 29%, 13%, 5%, 13%, 5% and 35%, respectively.
78 Fig. 1b shows the weight percentages of the main components in more recent LIBs
79 [14]. The cathode and anode together make up the highest proportion, 40% of the total
80 weight of LIBs. The two current collectors occupy the second-highest proportion with
81 a percentage of 15%, the electrolyte accounts for 11% and separator has the lowest
82 weight percentage of 4%. Other components, including case and tab, make up 30%
83 of the total weight. One observation is that the weight percentages of the current
84 collectors in LIBs has reduced slightly from 18% to 15% over the past two decades.

85 Current collectors can greatly influence the performance of LIBs. For example,
86 improving the electrical conductivity, reducing contact resistance and increasing the
87 corrosion resistance of current collectors are beneficial to increase the capacity, rate
88 capability, efficiency and cycle stability of LIBs [15]. Considering current collectors are
89 essentially non-active materials in LIBs, reducing the thickness of current collectors
90 can reduce the weight percentage and thus increase the energy density of LIBs.
91 Recent research pointed out that the thicknesses of Al and Cu current collectors are
92 reduced down to 10 μm for the pursuit of high energy density [16]. Nevertheless, thin
93 current collectors will sacrifice the electrical conductivity and heat transfer property of
94 current collectors and in turn power density. Therefore, there is a trade-off between
95 power and energy of LIBs in the design of these current collectors. Furthermore, as
96 electrodes are adhered to current collectors, mechanical integrity is also required in
97 current collectors in order to maintain a suitable bond to the electrodes during battery
98 cycling, this adhesive strength also contributes to the internal contact resistance of the
99 cell, and requires minimisation. More importantly, current collectors are indispensable
100 components for the present LIBs, any improvements in current collectors are expected
101 to benefit all LIBs. Fig. 1c displays a brief timeline of the development of current
102 collectors for LIBs in both industry and academia over the past three decades.

103 Many efforts have been made in reviewing cathodes, anodes, electrolytes and
104 separators of LIBs. However, to our knowledge, few reviews on current collectors have
105 so far been published and these only review limited materials or structures [17, 18].
106 This brings us to the need for a more comprehensive review of current collectors. This
107 paper attempts to review the development of various current collectors for LIBs in the
108 literature, including Al, Cu, Ni, Ti, stainless steel and carbonaceous materials. For Al
109 and Cu current collectors, we have further classified them into different categories

110 according to structures and treatments, namely foil, mesh, foam, etched and coated
 111 current collectors. Research challenges and future directions for current collectors are
 112 discussed at the end of this review.

113



114

115 Fig. 1 a) Schematic diagram of a typical Li-ion battery, b) the weight percentage of
 116 main components in LIBs [14], c) historical timeline of the development of current
 117 collectors for LIBs in both industry (yellow) and academia (red) [13, 16, 19, 20].

118 2. Main requirements for current collectors in lithium-ion batteries

119 a) Electrochemical stability. Current collectors must be electrochemically stable
 120 against oxidation and reduction environments during battery charging and
 121 discharging. In practice, a high voltage is favourable for increasing battery energy
 122 density, which requires that cathodes and anodes have high and low
 123 electrochemical potentials, respectively, e.g. LiCoO₂ cathode (~4 V vs Li/Li⁺) [21],

124 LiFePO₄ cathode (3.45 V vs Li/Li⁺) [22], and graphite anode (0.01 – 0.25 V vs Li/Li⁺)
125 [23]. However, it is challenging to keep current collectors stable when in direct
126 contact with electrolytes at such high and low potentials. Any undesired reactions
127 of current collectors may cause serious capacity fading and short service lifetimes
128 [24]. Therefore, good electrochemical stability is a prerequisite for all current
129 collectors. In this review, the electrochemical stability will be discussed first in each
130 section.

131 b) Electrical conductivity. All LIBs benefit from high electrical conductivity of current
132 collectors [25]. During battery cycling, electrons generated at the electrodes travel
133 through current collectors to external circuits. It is not only the conductivity of
134 current collectors that is crucial for LIB performance but also the electrode/current
135 collector interfacial conductivity. High electrical conductivity leads to low
136 transformation of chemical/electrical energy into heat during discharging/charging
137 process, contributing to high energy efficiency and capacity as well as avoiding the
138 risk of high temperatures.

139 c) Mechanical strength. Commercial electrodes in LIBs are fabricated by slurry
140 casting on metal foil current collectors [26]. The current collector serves as a
141 mechanical support for the electrode. Polymeric binder, usually polyvinylidene
142 difluoride (PVDF), is used to improve the integrity of the electrodes and adhesion
143 between electrodes and current collectors. Some electrodes undergo significant
144 volume change during cycling, which may cause serious electrode pulverisation or
145 delamination, particularly for thick electrodes. A typical example is Si anode which
146 suffers from up to 400% volume expansion due to the formation of LiSi alloy [27].
147 Current collectors with suitable levels of mechanical strength are helpful to
148 maintain the bonding of electrode active materials to the current collector and the
149 integrity of the whole electrodes during cycling.

150 d) Density. Conventional current collectors are non-active materials in LIBs as they
151 do not participate in electrochemical reactions during cycling. However, the current
152 collectors account for up to 20% of the total weight of LIBs. Using current collectors
153 with low densities is therefore favourable for reducing the overall weight of LIBs
154 and increasing the specific energy density of LIBs [28].

155 e) Sustainability and cost. The sustainable use of materials, in particular the critical
156 elements and strategic materials is crucial for the future of the battery industry. The
157 circular economic picture of cost, global availability and recyclability need to be

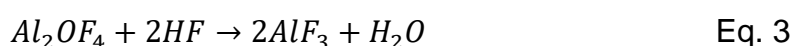
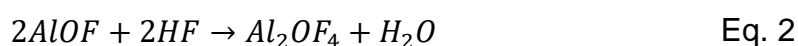
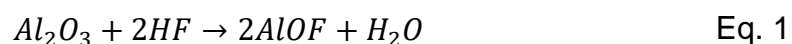
158 taken into consideration when we select and utilise materials for future current
159 collectors. Although cost is one of the most important concerns for
160 commercialization, what happens to the materials at end of the devices life also
161 needs consideration. The cost of current collectors may be reduced and the circular
162 economy of battery technologies improved by recycling current collectors from end-
163 of-life LIBs [29].

164 **3. Materials for current collectors**

165 **3.1 Al**

166 3.1.1 Electrochemical stability

167 The electrochemical behaviour of Al in the electrolyte of LiPF₆ in EC:DMC (1:1 vol.%)
168 was reported by Myung et al. [30], as shown in Fig. 2a. A cathodic peak at 0 V vs Li/Li⁺
169 and an anodic peak at 0.6 V vs Li/Li⁺ represent the alloying reaction between Al and
170 Li as well as the subsequent dealloying process, respectively. Two small anodic peaks
171 at about 3.7 and 4.7 V vs Li/Li⁺ result from the formation of a passivation film on Al
172 surface. Similar electrochemical behaviour of Al was reported previously [31]. The
173 current remains at about 0 mA cm⁻² as the potential moves to 5 V vs Li/Li⁺, indicating
174 good electrochemical stability. The good electrochemical stability is attributed to a
175 passivation film on Al surface, which consists of Al₂O₃ and AlF₃. The structure of this
176 passivation film was identified by Zhang and Devine [32]. As shown in Fig. 2b, the
177 passivation film consists of an air-formed Al₂O₃ layer with a thickness of 1.2 – 2.4 nm
178 on the bottom and a thin layer of AlF₃ with an estimated thickness of 1 nm on the top.
179 Myung et al. proposed a possible mechanism of the formation of AlF₃ [30]. As shown
180 in Eqs. 1 – 3, AlF₃ is derived from the reaction between Al₂O₃ and HF which is
181 generated from the decomposition of LiPF₆. Some factors, e.g. elevated temperature,
182 high potential and addition of H₂O, can facilitate the decomposition of LiPF₆, boosting
183 the formation of the AlF₃ passivation layer [33, 34],



184

185 The reactions stop when the AlF₃ passivation film is formed completely.[35]. The
186 electrochemical stability of Al is sensitive to both lithium salts and solvents. Similar to

187 LiPF₆, LiB(C₂O₄)₂ is another lithium salt which allows Al to form a passivation film of
188 AlBO₃ against corrosion [36]. Though Al shows excellent corrosion resistance in
189 electrolytes containing LiPF₆ and LiB(C₂O₄)₂, it is not stable in electrolytes containing
190 many other lithium salts, e.g. LiN(CF₃SO₂)₂, LiC(CF₃SO₂)₃, LiCF₃SO₃, and LiClO₄,
191 because the Al surface is only partially covered with AlF₃ [37, 38]. To this end, an
192 effective strategy is to use LiPF₆, LiBF₄, LiB(C₂O₄)₂, or LiBF₂(C₂O₄), as additives in
193 electrolytes to allow the formation of passivation films on the Al surface [39-43]. In
194 addition to lithium salts, solvents also have an effect upon the electrochemical stability
195 of Al, this is known to be related to their dielectric constant [44]. Solvents with low
196 dielectric constants are favourable, these exhibit limited solubility of the corrosion
197 products, instead of forming a protective layer adhered to the Al surface. Solvents with
198 high dielectric constants easily solvate the corrosion products removing them from the
199 current collector surface, diffusing into the bulk electrolyte. An example is using methyl
200 difluoroacetate (MFA) to replace EC:DMC (1:1 vol.%), which can improve the
201 electrochemical stability of Al current collectors [45]. It is noted however that the high
202 dielectric constant is beneficial for the dissociation of the lithium salts in the electrolyte,
203 and promotes fast ionic diffusion. Therefore again a trade-off between stability and
204 performance is observed.

205 The formation of passivation films on the Al surface enables Al to serve as the current
206 collector for cathodes. However, it is difficult to use Al for anodes because of the
207 alloying reaction between Al and Li at low potentials close to 0 V vs. Li/Li⁺. An
208 exception is Li₄Ti₅O₁₂ anode. Al current collectors can be used for Li₄Ti₅O₁₂ anodes
209 due to their high potentials, about 1.5 V vs. Li/Li⁺ [46].

210 3.1.2 Al foil

211 Al foils have been used as current collectors for cathodes since the first commercial
212 LIB which was developed by the Asahi Kasei team led by Yoshino and produced by
213 Sony in 1991 [47]. Apart from the excellent electrochemical stability already described,
214 high electrical conductivity is another advantage of Al foil current collectors. Al is the
215 fourth most conductive metal with an electrical resistivity of 2.65 x 10⁻⁸ Ωm at 20 °C,
216 following Ag, Cu and Au [48]. A common question is raised regarding the effect of the
217 insulating Al₂O₃ layer on the electrical conductivity of Al. Tian et al. measured the
218 electrical resistivity of an Al wire using the four-probe technique [49]. The Al wire was
219 not polished or subjected to any other treatments. Thus, an Al₂O₃ layer is expected to

220 form on the surface of the Al wire. The measured electrical resistance was 2.83×10^{-8} Ωm [49], which is very close to the value of pure Al. Similar work was done by Brandt
221 and Neuer who reported an electrical resistance of about 2.80×10^{-8} Ωm [50],
222 indicating that the Al_2O_3 layer does not affect the electrical conductivity of Al current
223 collectors.
224

225 Low density and good mechanical properties also make Al foils stand out from other
226 metals. Al has a low density of 2.70 g/cm^3 [48], which is favourable for increasing
227 battery gravimetric energy density. Early Al foil current collectors have a thickness of
228 $25 \mu\text{m}$, which are normally manufactured by rolling thicker stock foils into thinner and
229 thinner sheets [51]. The thickness of Al foil current collector was reduced down to 10
230 μm in further development to achieve high energy density. The effect of the thickness
231 of Al foils on LIB energy density can be seen by comparing two specific LIBs, Sony
232 VTC5A and VTC6 [16]. Both of the two Sony LIBs have an identical 18650 size, NCA
233 cathode, graphite and silicon composite anode. The VTC6 LIB has a thinner Al foil
234 with a thickness of $12 \mu\text{m}$, contributing to a higher gravimetric and volumetric energy
235 density of 246 Wh kg^{-1} and 665 Wh L^{-1} , respectively. While the counterpart (VTC5A
236 LIB) has a $15 \mu\text{m}$ thick Al foil, resulting in a lower gravimetric and volumetric energy
237 density of 196 Wh kg^{-1} and 552 Wh L^{-1} , respectively. However, the enhanced energy
238 density is at cost of power density. This is in part due to the thickness of the current
239 collectors, because the electrical conductivity and heat transfer property of Al foils
240 decrease with thickness, but also the thickness of the electrode films. This highlights
241 the interconnected electrode and cell engineering requirements that are required to
242 optimise the specific properties of a cell. The VTC5A LIB has a gravimetric and
243 volumetric power density of 2.3 kW kg^{-1} and 6.5 kW L^{-1} , respectively, higher than that
244 of the VTC6 LIB (1.6 kW kg^{-1} and 4.2 kW L^{-1}). The Al foil current collectors with a
245 thickness in the range of $10 - 20 \mu\text{m}$ have an estimated yield strength around 7 MPa
246 and tensile strength around 25 MPa at room temperature [52].

247 The price of commercial Al foil current collectors varies significantly with different
248 suppliers. To facilitate comparison with other materials in this study, we take the lowest
249 online quotation from an identical supplier, Goodfellow Cambridge Ltd., Huntingdon,
250 UK. The price of Al foil with a thickness of $20 \mu\text{m}$ and a high purity of 99% is about \$
251 $130/\text{m}^2$. It is worth mentioning that the price of Al foil from industrial suppliers is much
252 lower, with an estimated price of about \$ $5/\text{m}^2$ in 2011 [51].

253 3.1.3 Al mesh

254 The high contact resistance is a major issue of Al mesh current collectors. Arora et al.
255 reported the important role of the contact resistance between mesh current collectors
256 and electrodes in battery performance by simulations [53]. The contact resistance
257 mainly originates from the mesh current collector and ranges from 20 to 35 Ωcm^2 ,
258 depending on different cell specifications [53]. Hikmet conducted an experimental
259 study of the contact resistance between an Al mesh current collector and a LiCoO_2
260 cathode [54]. The electrical resistance of an Al mesh/ LiCoO_2 /Al mesh sandwich
261 structure is 40 Ω , which is equivalent to the resistance of two Al mesh/ LiCoO_2
262 interfaces. Given that the Al mesh current collector has a geometric surface area of
263 1.76 cm^2 , the resistance of the Al mesh/ LiCoO_2 interface can be converted into 35.2
264 Ωcm^2 , which agrees with Arora's work. Hikmet also measured the contact resistance
265 between a LiCoO_2 cathode and an Al film current collector which was directly
266 deposited on the LiCoO_2 cathode. The deposited Al/ LiCoO_2 interface has a resistance
267 of 1.32 Ωcm^2 , much lower than the Al mesh/ LiCoO_2 interface. The reason for this result
268 was not discussed by the author. We believe it is probably because of the different
269 electrode preparation process. Although the Al mesh and deposited Al film current
270 collectors have an identical geometric surface area, the cathode film was simply
271 pressed on the Al mesh current collector under heat, with poor adhesion resulting,
272 whereas the Al film current collector was deposited on the cathode film, resulting in a
273 higher contact area and thus lower contact resistance than the Al mesh current
274 collector.

275 Kanamura et al. compared the performance of $\text{LiNi}_{0.5}\text{Mn}_{1.5}\text{O}_4$ cathodes on Al mesh
276 and Al foil current collectors [55]. Both the Al mesh and foil current collectors produced
277 very similar initial discharge capacities of about 130 mAh g^{-1} , indicating a negligible
278 effect of the current collector. From the 2nd to 50th cycle, the Al mesh current collector
279 results in an average discharge capacity fade of 0.342 mAh g^{-1} per cycle, much higher
280 than the Al foil current collector with an average capacity fade of 0.0819 mAh g^{-1} per
281 cycle. The author ascribed the serious degradation in discharge capacity to the low
282 mechanical strength of the Al mesh which cannot withstand expansion and shrinkage
283 of the cathode during cycling.

284 Al meshes have also been used as current collectors for other cathodes, e.g.
285 $\text{LiAl}_y\text{Co}_{1-y}\text{O}_2$ [56], $\text{LiNi}_{0.5}\text{Mn}_{0.5}\text{O}_2$ [57], $\text{LiNi}_{0.8}\text{Co}_{0.2}\text{O}_2$ [58], $\text{Li}_3\text{Cr}_2(\text{PO}_4)_3$ [59]. However,

286 the benefits and drawbacks of Al mesh current collectors were not well discussed in
287 these studies.

288 3.1.4 Al foam

289 Al foams have been used as current collectors for LIBs due to the unique porous
290 structures that enable high electrode mass loading. For conventional Al foil current
291 collectors, high electrode mass loading is challenging because of the high risk of
292 electrode delamination during cycling. An ultra-thick Al foam current collector with a
293 thickness of 258 μm was used for $\text{LiNi}_{0.33}\text{Mn}_{0.33}\text{Co}_{0.33}\text{O}_2$ cathodes by Fritsch and his
294 colleagues [60]. The Al foam current collector allows high electrode mass loadings of
295 electrode active material up to 42 mg cm^{-2} and thus high capacities up to 7 mAh cm^{-2} ,
296 more than three times higher than commercial $\text{LiNi}_{0.33}\text{Mn}_{0.33}\text{Co}_{0.33}\text{O}_2$ cathodes with
297 a thickness around 50 μm on a conventional Al foil current collector ($\sim 12 \text{ mg cm}^{-2}$
298 loading and $\sim 2 \text{ mAh cm}^{-2}$ capacity) [61]. It should be noted that the electrode mass
299 loading on Al foam current collectors also depends on loading techniques. The
300 aforementioned high mass loading is achieved by slurry infiltration under vacuum. For
301 example, another sample prepared by dip-coating on an Al foam current collector with
302 a similar thickness, only has a mass loading of 7.8 mg cm^{-2} and low capacity of 1.24
303 mAh cm^{-2} . Although the two samples prepared by two different loading processes have
304 different areal capacities, they have very similar gravimetric capacities in the range of
305 160 – 170 mAh g^{-1} , implying that they have a similar electrode efficiency. Therefore, Al
306 foam current collectors can increase only absolute or areal capacity but not gravimetric
307 capacity. Compared with Al foils, the Al foams also contribute to a much lower charge
308 transfer resistance at the electrode/electrolyte interface, further improving the
309 electrode performance [60].

310 Al current collectors with porous structures are also beneficial to increase Li-ion
311 diffusion during cycling. Li-ion diffusion within electrodes has been regarded as the
312 rate-determining step for LIB cycling, particularly at high current densities [62]. Du et
313 al. prepared an Al current collector with tunnel-like pores for TiO_2 anodes [63], as
314 shown in Fig. 2c and d. The tunnel-pores provide not only a high surface area for TiO_2
315 loading but also a diffusion pathway for Li-ions during cycling. The enhanced Li-ion
316 diffusion enables fast charging/discharging. The TiO_2 anode on the porous Al current
317 collector delivers a capacity of 95 mAh g^{-1} at a very high current rate of 100 C and
318 remains stable after 8000 cycles.

319 3.1.5 Etched Al

320 Chemical etching is a treatment for current collectors to achieve a rough surface and
321 better performance. Nakamura et al. investigated the effect of the surface morphology
322 of Al current collectors on the electrochemical performance of
323 $\text{LiCo}_{0.33}\text{Ni}_{0.33}\text{Mn}_{0.33}\text{O}_2$ cathodes [64]. Two different Al current collectors, one with and
324 the other one without surface treatment, were employed in the study. The treatment
325 process was probably chemical etching, judging by the surface morphology of the
326 treated Al current collector which is covered by numerous sub-micron-sized pores,
327 although the author only mentioned this as 'chemical treatment'. The surface-modified
328 Al current collector leads to almost the same capacities as the normal Al current
329 collector at current rates smaller than 1 C, but higher capacities at higher current rates,
330 due to improved contact resistance. Besides this, the surface-modified Al current
331 collector also contributes to higher capacity retention after 30 cycles. Yoon et al.
332 investigated the effect of the surface morphology of Al current collectors on the
333 electrochemical performance of LiCoO_2 cathodes [65]. Two type solutions, i.e. a
334 mixture of NaOH, Na_2CO_3 , $\text{C}_6\text{H}_{11}\text{NaO}_7$ and a mixture of NaOH, NaNO_3 , $\text{C}_6\text{H}_{11}\text{NaO}_7$,
335 were employed to obtain different Al surface morphology after different etching time
336 between 10 – 70 s. The etched Al foil with the roughest surface exhibits the highest
337 discharging capacity, particularly at high current rates, up to 4 times higher than a
338 normal Al foil current collector. The superior electrochemical performance of the
339 surface-modified Al current collector arises from the rough surface which increases
340 the adhesion between the current collectors and electrodes as well as reduces the
341 charge transfer resistance of the LiCoO_2 cathode. The strong adhesion further avoids
342 peeling of the electrode and maintains low contact resistance. Additionally, chemical
343 etching slightly decreases the tensile strength but increases the surface hydrophilicity
344 of Al current collectors [65].

345 Nakanishi et al. reported that the enhancement effect of etched Al current collectors
346 on electrode performance is also affected by electrode type and active material particle
347 size [66]. LiCoO_2 cathodes with large particles on a normal and etched Al foil current
348 collector show similar performance, while LiFePO_4 cathodes with small particles
349 exhibit highly increased discharge capacities when using an etched Al current collector
350 to replace a normal Al foil current collector. However, based on these results, it is not
351 possible to confidently solely ascribe the difference to either the effect of electrode

352 type or material particle size. The author also quantitatively measured the peel
353 strength between the LiFePO₄ cathode and current collectors. The etched Al current
354 collector gives rise to a 7 times stronger bond to the cathode than the normal Al current
355 collector.

356 Due to enhanced adhesion and electrical conductivity of etched Al current collectors,
357 Shin et al. proposed to use an etched Al current collector for LiCoO₂ cathodes in
358 ultrafast LIBs [67]. The LiCoO₂ cathode on the etched Al current collector exhibits an
359 initial capacity of 90 mAh g⁻¹ at a high current rate of 10 C with 85% retention after 250
360 cycles. For comparison, the LiCoO₂ cathode on a normal Al current collector cannot
361 work properly at such a high current rate.

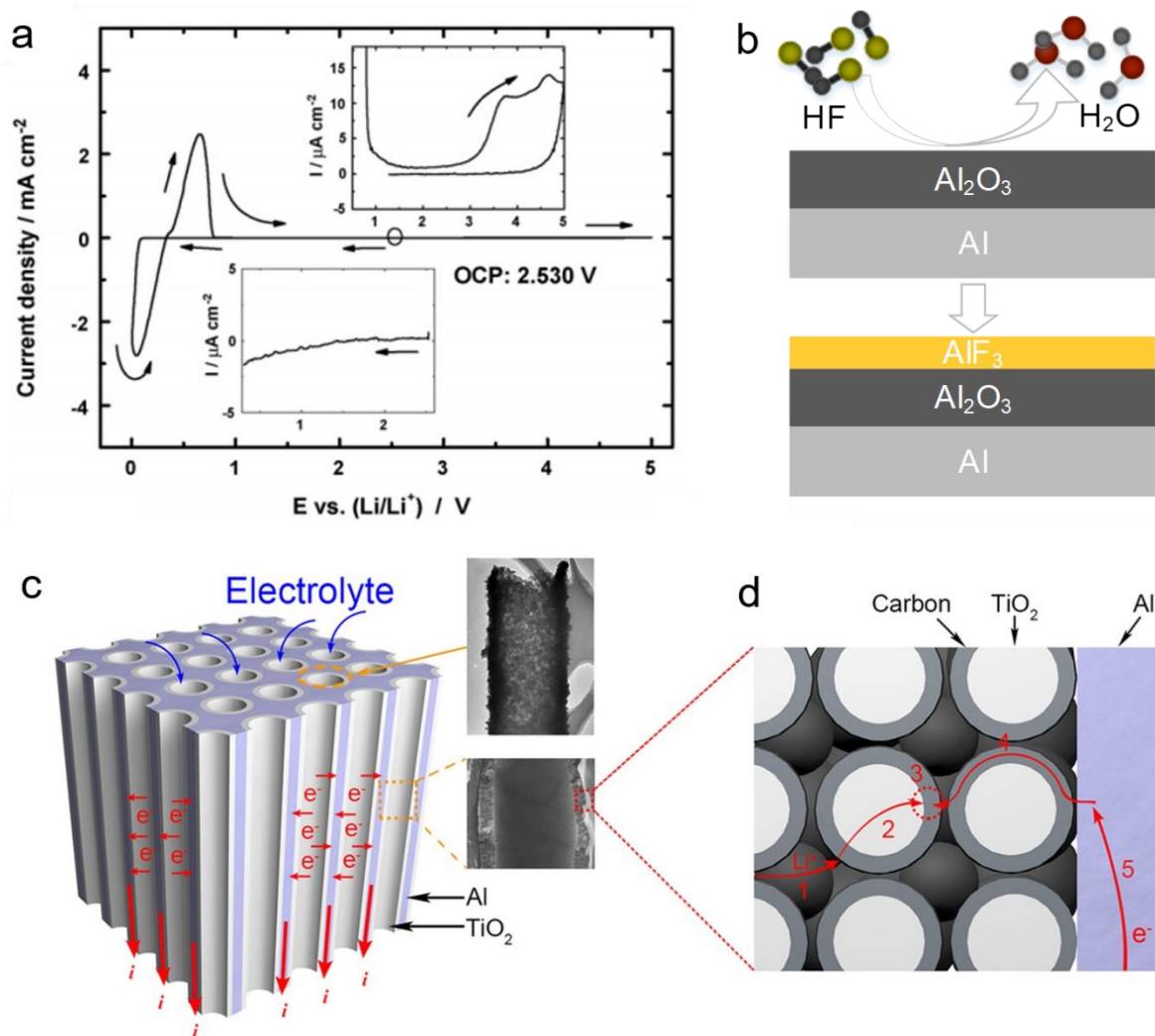
362 3.1.6 Coated Al

363 Coating is an effective way to improve the conductivity of Al current collectors to
364 achieve better electrode performance. Striebel et al. compared the performance of
365 LiFePO₄ cathodes on a carbon-coated and a bare Al current collector [68]. The
366 LiFePO₄ cathode on the carbon-coated Al current collector delivers a discharge
367 capacity of 160 mAh g⁻¹ at a low current rate of 0.2 C and has a 70% capacity retention
368 at a high current rate of 5 C, while the LiFePO₄ cathode on the bare Al current collector
369 delivers a discharge capacity of 140 mAh g⁻¹ at 0.2 C and only has a 15% capacity
370 retention when the current rate increases to 5 C. The LiFePO₄ cathode on the bare Al
371 current collector also undergoes serious voltage drop from 3.4 to ~2.6 V vs. Li/Li⁺ as
372 the charging rate increases from 0.2 C to 5 C, indicating that the bare Al current
373 collector brings a large contact resistance. Replacing the bare Al current collector with
374 the carbon-coated Al current collector gives rise to a contact resistance drop from 200
375 to ~40 Ωcm² and thus a small voltage drop of 0.2 V when the charging rate increases
376 from 0.2 C to 5 C. Furthermore, the formation of carbon coating on Al current collectors
377 in flowing CH₄ at 600 °C can remove the native oxide on the Al surface and thus
378 improve electrical conductivity [69].

379 Coating can also improve the corrosion resistance of Al current collectors. Doberdò et
380 al. used a carbon-coated Al current collector for LiNi_{0.33}Mn_{0.33}Co_{0.33}O₂ cathodes with
381 carboxymethyl cellulose (CMC) as a binder and water as a solvent [70]. Though
382 normal Al current collectors suffer from serious corrosion when in direct contact with
383 this LiNi_{0.33}Mn_{0.33}Co_{0.33}O₂ cathode slurry due to its basicity, the carbon-coated Al

384 current collector shows good corrosion resistance. The thickness of the carbon coating
385 is crucial for corrosion resistance. For the Al surface coated with a 2 μm carbon layer,
386 small corrosion pits were still visible, while no evident trace of corrosion was observed
387 on the Al surface coated with a 5 μm carbon layer. The $\text{LiNi}_{0.33}\text{Mn}_{0.33}\text{Co}_{0.33}\text{O}_2$ cathode
388 on the 5 μm carbon-coated Al current collector delivers a capacity of 126 mAh g^{-1} at 1
389 C after 50 cycles, higher than an identical cathode on a normal Al current collector
390 (107 mAh g^{-1}).

391 Apart from carbon, other materials have also been coated on Al current collectors to
392 improve electrode performance, e.g. graphene oxide [71], Mn and Al oxide composite
393 [72], chromate [73] and graphene [74]. All of these coatings are reported to be
394 favourable for improving either or both of the electrical conductivity and
395 electrochemical stability of Al current collectors. Among them, the Mn and Al oxide
396 composite and graphene coatings can also improve the adhesion between Al current
397 collector and electrodes.



398

399 Fig. 2 a) Cyclic voltammety of Al in 1 M LiPF₆ in EC:DMC (1:1 vol.%) electrolyte
 400 (Reproduced with permission [30]. Copyright 2009 Elsevier), b) schematic drawing of
 401 passivation film formed on Al surface, c) and d) tunnel-like Al foam current collector
 402 (enlarged view: 1 ion transport in the electrolyte, 2 ion transport in the electrode, 3
 403 electrochemical reactions in the electrode, 4 electron transport in the electrode and 5
 404 electron conduction in the current collector) [63].

405 **Table. 1 Al current collectors**

Type	Electrode	Current rate/C	Capacity/ mAh g ⁻¹	Capacity retention (cycles)	Reference
Foil	LNMO	0.1	130	97% (50)	[55]
Foil	NMC111	0.1	178	91% (30)	[64]
		10	20	-	

Foil	LCO	~0.1	188	93% (50)	[65]
		~2.7	25	-	
Foil	LCO	0.2	142	-	[66]
		1	138	-	
		5	96	-	
Foil	LFP	0.2	128	-	[66]
		1	105	92% (240)	
		5	0	-	
Foil	LCO	1	120	71% (100)	[67]
		10	0	-	
Foil	LFP	0.2	140	-	[68]
		5	20	-	
Foil	NMC111	1	110	97% (50)	[70]
		10	35	-	
Foil	LMO	3	100	80% (100)	[71]
Foil	LFP	0.1	158	-	[72]
		1	145	84% (2000)	
		5	116	-	
Foil	LMO	-	130	0% (50)	[73]
Foil	LCO	0.1	150	-	[74]
		1	130	4% (50)	
		5	45	-	
Mesh	LNMO	0.1	130	87% (50)	[55]
Mesh	LNMO	0.1	174	~100% (10)	[57]
		0.5	145	90% (40)	
		2	110	-	
Foam	NMC111	0.2	166	90% (140)	[60]
		2	55	-	
Foam	TiO ₂	0.3	330	-	[63]
		100	100	~100% (8000)	
Etched	NMC111	0.1	178	94% (30)	[64]
		10	25	-	
Etched	LCO	~0.1	190	96% (50)	[65]
		~2.7	125	-	

Etched	LCO	0.2	140	-	[66]
		1	138	-	
		5	104	-	
Etched	LFP	0.2	125	-	[66]
		1	114	~100% (240)	
		5	80	-	
Etched	LCO	1	135	85% (100)	[67]
		10	90	85% (250)	
Carbon-coated	LFP	0.2	160	-	[68]
		5	110	-	
Carbon-coated	NMC111	1	120 (2 μm) ^a	97% (50)	[70]
			128 (5 μm) ^a	98% (50)	
		10	51 (2 μm) ^a	-	
			60 (5 μm) ^a	-	
Graphene oxide-coated	LMO	3	100	90% (100)	[71]
Mn and Al oxide composite-coated	LFP	0.1	162	-	[72]
		1	150	95% (2000)	
		5	120	-	
Chromate-coated	LMO	-	115	87% (50)	[73]
Graphene-coated	LCO	0.1	160	-	[74]
		1	135	55% (50)	
		5	110	-	

406 Note: partial data were taken from published figures by approximation, ‘-’ means data
407 not given, as noted for other tables.

408 ^a denotes current collectors with specific coating thicknesses.

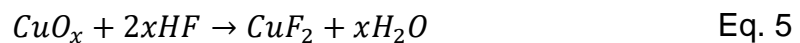
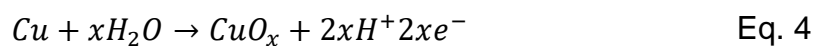
409 3.2 Cu

410 3.2.1 Electrochemical stability

411 The electrochemical behaviour of Cu in the electrolyte of LiPF₆ in EC:DMC (1:1) is
412 shown in Fig. 3a. An open circuit potential at 3.326 V vs Li/Li⁺ is initially observed, the
413 first cathodic peak can be seen at about 3.1 V vs Li/Li⁺, which is suggested to
414 correspond to the decomposition of LiPF₆ to HF [75]. A large cathodic peak is observed
415 between 1.5 – 3 V vs Li/Li⁺, which corresponds to the reduction process of the air-
416 formed Cu oxide film to metal, the electrolytic salt formation of Li₂O, the reduction of

417 the solvent and the formation of the solid electrolytic interphase (SEI) layer on the Cu
 418 surface [30, 44]. A small cathodic peak and anodic peak at about 0.6 V and 0.7 V vs
 419 Li/Li⁺ represent underpotential deposition of Li on the Cu surface and subsequent
 420 dissolution of the deposited Li in the electrolyte, respectively [30, 44]. As Cu is
 421 polarized in the anodic direction, no other peak appears until approaching a high
 422 potential of 3.5 V vs Li/Li⁺. The anodic peak at about 3.7 V vs Li/Li⁺ has been identified
 423 as the dissolution of Cu into the electrolyte [30, 44]. Similar dissolution behaviours of
 424 Cu in other electrolytes of LiPF₆ in EC:DEC (1:1 vol.%), LiClO₄ in EC:DEC(1:1 vol.%)
 425 and LiClO₄ in PC at high potentials were also reported by Iwakura et al. [76] and
 426 Kawakita et al. [77]. The dissolution of Cu can cause numerous pits with a
 427 characteristic shape which looks like a hole with the square aperture area advanced
 428 toward the inside of the substrate, as shown in Fig. 3b. Therefore, the dissolution of
 429 Cu is also named ‘pitting corrosion’ in many studies.

430 A small amount of water and HF can boost the dissolution of Cu [78]. The mechanism
 431 was proposed by Dai and his colleagues [79]. As shown in Eqs. 4 – 5, Cu is first
 432 oxidized by water with the formation of Cu oxide. The Cu oxide further reacts with HF
 433 either generated from the decomposition of LiPF₆ or introduced externally, producing
 434 CuF₂. Both CuO and CuF₂ have been proven to exist on the Cu surface after
 435 immersion in the electrolyte of LiPF₆ in EC:DMC (1:1 vol.%) [30, 44]. Nevertheless,
 436 they do not form a substantial passivation film on the Cu surface. The dissolution of
 437 Cu can also be affected by electrolytes. It was found that Cu is more readily dissolved
 438 in the solvent of PC:EC:DMC (1:1:3 vol.%) than EC:DMC:DEC (2:2:1 vol.%) and
 439 EC:DMC:MEC (1:1:1 vol.%) at the same potentials [78]. However, the reason is still
 440 not clear.



441 Though the dissolution of Cu at high potentials hinders Cu serving as the current
 442 collector for cathodes, the stable electrochemical behaviour of Cu at potentials below
 443 3 V vs Li/Li⁺ as well as no alloying reactions with Li make Cu a good choice for current
 444 collectors at anodes because most anodes have low potentials. However, over-
 445 discharging may raise the potential of anodes, causing severe Cu dissolution. The
 446 dissolved Cu ions will redeposit as Cu metal at anodes to form dendrites and pierce

447 the separator, resulting in capacity fading and short-circuit of LIBs [80]. Therefore,
448 over-discharging should be avoided when using Cu current collectors for anodes.

449 3.2.2 Cu foil

450 Almost all commercial LIBs use Cu foils as current collectors for anodes since the first
451 LIB produced by Sony [47]. The initial Cu foils were manufactured by rolling and
452 therefore low levels of oil were present upon the surface, this caused adhesion issues,
453 and therefore needed to be removed before use [81]. More recently Cu foils are
454 manufactured by electrodeposition methods [82]. Apart from the good electrochemical
455 stability aforementioned, Cu is the second most conductive metal with a resistivity of
456 $1.68 \times 10^{-8} \Omega\text{m}$ at 20°C [48], which is another advantage of using Cu current collectors.
457 However, Cu is much heavier than Al with a density of 8.96 g/cm^3 [48]. The high density
458 of Cu results in Cu foil current collectors occupying more than 10% of the total weight
459 of LIBs, about twice of the Al foil current collector for cathodes [13].

460 Similar to Al foil current collectors, Cu foil current collectors tend to be thinner and
461 thinner for the pursuit of high energy density [16]. Two specific LIBs, Samsung 30Q
462 and Sony VTC5A, have an identical battery size, cathode and anode, as well as very
463 similar battery design. The Samsung 30Q LIB has a $10 \mu\text{m}$ Cu foil current collector,
464 thinner than the Sony VTC5A ($14 \mu\text{m}$). The Samsung 30Q LIB has a gravimetric and
465 volumetric energy density of 245 Wh kg^{-1} and 657 Wh L^{-1} , respectively, higher than
466 the Sony VTC5A (196 Wh kg^{-1} and 552 Wh L^{-1}). However, the thinner Cu foil current
467 collector and coated electrodes of the Samsung 30Q LIB results in a lower gravimetric
468 and volumetric power density of 1.2 kW kg^{-1} and 3.2 kW L^{-1} , respectively, compared
469 with the Sony VTC5A having a gravimetric and volumetric power density of 2.3 kW kg^{-1}
470 and 6.5 kW L^{-1} . This highlights, similar to the aluminium current collector and
471 cathode, that the combination of electrode and cell design is important when
472 optimising the performance properties of a cell.

473 Special concern has been expressed over the mechanical strength of Cu foil current
474 collectors because Cu foils may suffer from environmentally assisted cracking and
475 structure degradation during repeated battery cycling under bending stress [34].
476 Recent work also reported that Cu foil current collectors for Sn-based anodes
477 underwent structural degradation during cycling [83]. The mechanical properties of
478 commercial Cu foil current collectors were systematically investigated by Zhu and his

479 colleagues [84]. The elastic modulus, tensile, fracture and yield strengths of Cu foils
480 with a thickness of 8 – 35 μm are in the ranges of 45 – 75 GPa, 300 – 350 MPa, 260
481 – 360 MPa and 40 – 180 MPa, respectively, which is higher than that of Al foils.

482 At the time of writing, the cost of Cu foils with a thickness of 20 μm and a purity of
483 99.9% is about \$ 640 / m^2 , from the online quote of Goodfellow, much higher than that
484 of Al foils.

485 3.2.3 Cu mesh

486 Li et al. used Cu meshes as current collectors for Li metal anodes [85]. To connect the
487 Cu mesh current collector and Li metal anode, a circle-shaped copper mesh with a
488 pore diameter in the range of 60 – 170 μm was aligned with a Li metal foil and pressed
489 with a punching machine until the Cu mesh was fully embedded in the Li metal. The
490 Li metal anode on the Cu mesh current collector exhibits much better cycling
491 performance than that on a conventional Cu foil current collector, with a high
492 coulombic efficiency of 93.8% after 100 cycles against a low coulombic efficiency of
493 30.9% after 70 cycles at a current rate around 0.5 C, respectively. When used in a Li/
494 $\text{Li}_4\text{Ti}_5\text{O}_{12}$ cell, the Li metal anode on the Cu mesh current collector results in a higher
495 cell capacity than a bare Li metal anode, particularly at high current rates. The
496 enhanced performance of the Cu mesh current collector can be attributed to four
497 aspects. 1) the presence of holes on the Cu mesh enhances the charge transfer
498 kinetics and reduces the electrode/electrolyte interfacial resistance. Li anode on the
499 Cu mesh current collector has a low electrode/electrolyte interface resistance of 27
500 Ωcm^2 after 10 cycles, while a bare Li anode shows a high interface resistance of 62
501 Ωcm^2 . 2) The Cu mesh current collector can accommodate the volume change of Li
502 anode to some extent during battery cycling. This unique function also makes Cu mesh
503 a good current collector for Si-based anodes that suffer from severe volume change
504 [86, 87]. 3) The high surface area of Cu meshes lowers the areal current density,
505 leading to uniform charge distribution and thus smoothening the Li deposition and
506 preventing Li dendrite formation [88]. 4) The thickness of the anode remains almost
507 unchanged during cycling, providing good mechanical stability of the anode and
508 integrity of cells.

509 3.2.4 Cu foam

510 Cu foams can bring many benefits when used as current collectors, particularly for Li
511 metal anodes that have high theoretical capacity but suffer from severe volume
512 change and Li dendrite formation. The porous structure of Cu foams can greatly
513 accommodate the volume expansion/contraction of Li metal anodes during cycling.
514 Besides, Cu foams provide much higher surface areas than Cu foils, which lowers the
515 local current density and in turn prevents Li dendrite formation. Therefore, Cu foams
516 are ideal current collectors for Li metal anodes from this point of view. A typical
517 example of using Cu foams as current collectors to improve Li anode performance is
518 reported by Yun and his colleagues [89]. They fabricated Cu foams with a pore size in
519 the range of 0.2 – 2 μm by chemical dealloying of CuZn. The as-fabricated Cu foam
520 current collector results in a coulombic efficiency over 95% at 1 C after 150 cycles,
521 much better than a conventional Cu foil current collector with a coulombic efficiency of
522 80% under the same measurement conditions. Similar conclusions have also been
523 drawn from other studies [90, 91].

524 Cu foam current collectors with pores neither too big nor small are appropriate for
525 improving Li metal anode performance. Small pores, e.g. nano-sized pores, can
526 prevent Li dendrite formation due to high surface area but suffer from the volume
527 change of Li metal anodes. By contrast, large pores, e.g. micron-sized pores, can
528 accommodate the volume change but only provide limited surface area. Liu et al.
529 developed a hierarchical Cu foam current collector with both micron- and nano-sized
530 pores for Li metal anodes, providing a good solution for this problem. The micron- and
531 nano-sized pores are formed by physical dealloying and immersion in a NaOH and
532 $(\text{NH}_4)_2\text{S}_2\text{O}_8$ mixed solution, respectively. The micron-sized pores effectively
533 accommodate the volume change of the Li metal anodes during cycling and the nano-
534 sized pores increase total surface area and prevent Li dendrite formation [92]. The
535 surface area of a hierarchical Cu foam containing both micron- and nano-sized pores
536 can be up to 60 times higher than that of a Cu foam only containing micron-sized pores
537 [93]. The as-produced hierarchical Cu foam results in a high coulombic efficiency more
538 than 98% at 1 mA cm^{-2} after 200 cycles, better than a Cu foam only with micron-sized
539 pores (90% after 200 cycles) and a conventional Cu foil (23% after 150 cycles).

540 The pore geometry is also key for Cu foam current collectors. Wang et al. developed
541 a Cu foam current collector with vertically aligned microchannels for Li metal anodes

542 [94]. The vertically aligned microchannels exhibit a tip effect, leading to preferential
543 nucleation of Li inside the mouth of channels and preferential deposition on the
544 microchannel walls and thus effectively restraining growth of Li dendrites. The tip effect
545 essentially means the surface with a high curvature has high surface potential due to
546 the distortion of the electrical field, which makes Li dendrites form more readily [95].
547 The geometry of the microchannels, i.e. radius, depth and spacing, can also affect
548 battery performance. With optimised microchannel geometry, the Li anode on the
549 vertically aligned microchannels current collector exhibits a high stable coulombic
550 efficiency around 98.5% at 1 mA cm^{-2} within 200 cycles, much better than conventional
551 Cu foil current collectors with a coulombic efficiency dropping from 98% in the 1st cycle
552 to 50% after 80 cycles. Wang et al. fabricated Cu foam current collectors through a
553 NaCl-assisted powder sintering process [96]. The produced Cu foam has
554 interconnected micron-sized pores with a smooth inner surface, which provides high
555 surface area and facilitates Li-ions diffusion, resulting in uniform Li deposition and
556 effectively suppressing Li dendrite formation. The as-fabricated interconnected Cu
557 foam contributes to a coulombic efficiency higher than 90% at 1 mA cm^{-2} after 400
558 cycles. For comparison, the commercial Cu foams manufactured by electrodeposition
559 only results in a coulombic efficiency of 50% at 1 mA cm^{-2} after 300 cycles.

560 Cu foam current collectors can also bring many benefits to other anodes apart from Li
561 metal anodes. For example, Cu foams with a porosity of 97% enable fabrication of
562 thick graphite anodes with a thickness of up to 1.2 mm which is 10 times greater than
563 conventional Cu foils [97]. The thick graphite anode greatly improves the energy
564 density of LIBs but sacrifices the observed gravimetric capacity due to increased
565 internal resistance. The gravimetric capacity of the graphite anode decreases from
566 375 to 275 mAh g^{-1} as the electrode thickness increases from 0.3 to 1.2 mm. The
567 author solely ascribed the reduced gravimetric capacity to increased electronic
568 resistance, which is evidenced by the result that the voltage hysteresis between the
569 charge and discharge is smaller for the thinner electrode. We believe not only the
570 electronic resistance but also Li-ion diffusion reduces the gravimetric capacity of thick
571 electrodes. Because the thick electrode is difficult for Li-ions to diffuse through and
572 can cause Li-ion depletion in the electrolyte phase [98]. Additionally, Cu foams can
573 effectively accommodate the volume change of Si and Sn anodes during battery
574 cycling [99, 100]. When used as current collectors for Sn anodes, the phase

575 transformation of Sn into Cu_6Sn_5 takes place on the electrode/current collector
576 interface. The newly-formed phase Cu_6Sn_5 enhances the bonding force between Sn
577 anodes and Cu foam current collectors, further restraining the volume changes of
578 active materials during cycling [100].

579 3.2.5 Etched Cu

580 Cu current collectors with a rough surface are favourable to improving electrode
581 performance [101, 102]. Nguyen et al. used an etched Cu current collector for
582 amorphous Si anodes [103]. The rough surface of the etched Cu provides a high
583 contact area and thus strong adhesion to the Si anode as well as good electrical
584 conductivity. Meanwhile, the etched holes existing on the surface are filled up with Si,
585 indicating a higher mass loading than Cu foils. With the help of a siloxane-stabilized
586 electrode/electrolyte interface, the Si anode on the etched Cu current collector exhibits
587 a discharge capacity up to 4255 mAh g^{-1} , versus 2428 mAh g^{-1} for the Si anode on an
588 unetched Cu current collector. The discharge capacities of the Si anodes on the
589 etched and unetched Cu current collectors remain at 80% and 53% after 200 cycles,
590 respectively. A similar study was conducted by Reyter and his colleagues who used
591 etched Cu current collectors for Si powder anodes [104]. The etched Cu contributes
592 to a high capacity up to 2410 mAh g^{-1} at 600 mA g^{-1} after 25 cycles versus 1630 mAh
593 g^{-1} for an unetched Cu current collector. They also quantitatively compared the
594 adhesion strength between the Cu current collectors and Si anodes through a scratch
595 test. The minimum load in grams required to scrape through the Si anode to the etched
596 and unetched Cu current collectors are 110 and 40 g, respectively, proving that the
597 etched surface provides a stronger adhesion to the Si anode.

598 Selective etching on Cu current collectors can effectively alleviate the volume change
599 of Si anodes during cycling. Cho et al. selectively etched Cu foils with discontinuous
600 lines at regular spacings and subsequently deposited Si on the etched Cu current
601 collectors to obtain discontinuous Si anodes [105]. The discontinuous Si anode
602 exhibits better cycle stability than continuous Si anodes, i.e. Si deposited on a
603 conventional Cu foil current collector. The enhanced cycle stability is attributed to the
604 discontinuous lines that accommodate the stress generated by the volume change of
605 Si anodes. Three different spacings between the discontinuous lines of 400, 800, 1700
606 μm were made to investigate the effect of spacing, with the smallest spacing of 400
607 μm resulting in the best performance. Cho et al. further developed trench-structured

608 Cu current collectors for Si anodes following a similar selective etching and deposition
609 process [106]. Si film was deposited on either the whole surface of the etched Cu
610 current collector or only the bottom of the trenches, termed wholly covered Si film
611 anode or selectively covered Si film anode, respectively, as shown in Fig. 3c-e. The
612 wholly covered Si anode exhibits an 18.5% increase in initial capacity compared to the
613 continuous Si film anodes. The selectively covered Si film anode shows even better
614 performance than the wholly covered one. The geometry of the etched trenches has
615 modest effects on the Si anode performance, with a trench width of 45 μm and trench
616 height of 14 μm resulting in the highest columbic efficiency and best cycle performance.

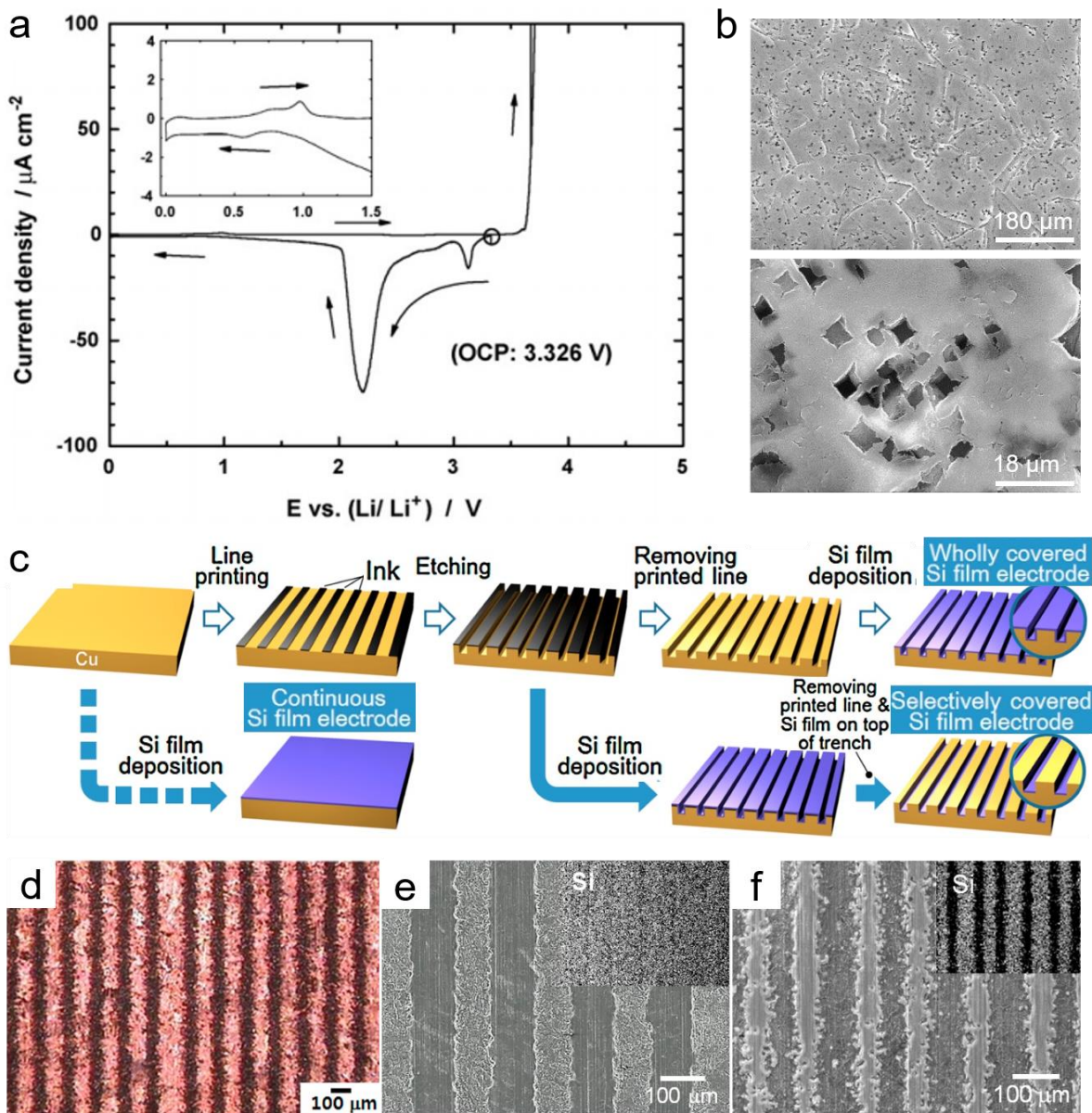
617 3.2.6 Coated Cu

618 Cu current collectors with various material coatings can provide many benefits. Kang
619 et al. coated conventional Cu foils with a rough layer of carbon via an electric discharge
620 method and used the carbon-coated Cu foils as current collectors for graphite anodes
621 [107]. The carbon-coated Cu current collector shows reduced electrical and charge
622 transfer resistance, resulting in higher capacity and better rate capability than
623 conventional Cu foil current collectors. Wu et al. prepared carbon-coated Cu current
624 collectors via chemical vapour deposition at 600 $^{\circ}\text{C}$ and subsequently used the as-
625 prepared current collectors for $\text{Li}_4\text{Ti}_5\text{O}_{12}$ anodes [69]. In addition to improved electrical
626 and charge transfer properties, the carbon-coated Cu current collector prepared at
627 high temperature shows greater surface hydrophobicity than conventional Cu foils,
628 which improves the surface adhesion to the $\text{Li}_4\text{Ti}_5\text{O}_{12}$ anode. More importantly,
629 $\text{Li}_4\text{Ti}_5\text{O}_{12}$ anode is known to have a high voltage plateau at about 1.55 V vs Li/Li^+ during
630 cycling, which is challenging for Cu current collectors due to low corrosion resistance
631 at high potentials. The carbon coating is expected to provide a protective film for Cu
632 against corrosion, leading to improved cycle stability. Similar benefits can also be
633 found from graphene-coated Cu current collectors [108]. The graphene coating on Cu
634 current collectors brings up to 32% increase in the capacity of $\text{Li}_4\text{Ti}_5\text{O}_{12}$ anodes due
635 to enhanced electrical conductivity, charge transfer kinetics, adhesion to anodes and
636 electrochemical stability.

637 Coating is an effective way to make the surface of current collectors lithiophilic. Zhang
638 et al. constructed a Cu current collector coated with vertically aligned CuO nanosheets
639 via NH_4OH etching for Li metal anodes [109]. The Li metal anode on the CuO-coated
640 Cu current collector provides a high coulombic efficiency of 94% at a current density

641 of 1 mA cm^{-2} for 180 cycles, in contrast to a conventional Cu current collector with a
642 coulombic efficiency less than 20% after 150 cycles. A prolonged lifespan of 700 h at
643 0.5 mA cm^{-2} is also easily achieved. The enhanced performance arises from the
644 lithiophilic CuO coating which can reduce the nucleation overpotential and guide
645 uniform Li nucleation and deposition [110]. Ag is another lithiophilic material which has
646 been used to coat Cu current collectors [111]. The Li metal anode on the Ag-coated
647 Cu foil exhibits a stable coulombic efficiency of 98% for 50 cycles at a current density
648 of 1 mA cm^{-2} versus 95% for 20 cycles for uncoated Cu foils. The Ag-coated Cu
649 current collector results in an improved lifespan of up to 360 h at 1 mA cm^{-2} , more
650 than twice of the uncoated Cu foil current collector. Other materials, such as Ni and
651 ZnO, can also be coated to make the Cu surface lithiophilic [112, 113]. It is worth
652 mentioning that the Li metal anodes also benefit from the nanostructures of CuO and
653 Ag which can facilitate fast Li-ion diffusion and reduce the local current density.

654 Artificial SEI can also be directly coated on Cu current collectors to improve electrode
655 performance. Luo et al. coated Cu current collectors with a thin layer of high-polarity
656 β -PVDF for Li metal anodes [114]. The β -PVDF has all trans conformation with F and
657 H atoms located on the opposite sides of the polymer backbone, serving as an artificial
658 SEI to facilitate uniform Li deposition by the strong interactions between its polar
659 functional groups and Li-ions. The β -PVDF-coated Cu current collector enables
660 uniform Li deposition/stripping at high current densities up to 5 mA cm^{-2} , Li-plating
661 capacity loadings of up to 4 mAh cm^{-2} , and excellent cycling stability over hundreds
662 of cycles.



663

664 Fig. 3 Cyclic voltammetry of Cu in 1 M LiPF₆ in EC:DMC (1:1 vol.%) electrolyte
 665 (Reproduced with permission [30]. Copyright 2009 Elsevier), b) pitting corrosion on Cu
 666 surface (Reproduced with permission [77]. Copyright 2001 Elsevier), c) fabrication
 667 process for continuous, wholly covered and selectively covered Si film anodes, d)
 668 etched Cu current collector, e) wholly covered Si film anode, f) selectively covered Si
 669 film anode, c-f from (Reproduced with permission [106]. Copyright 2017 Elsevier).

670 **Table. 2 Cu current collectors**

Type	Electrode(s)	Current rate/C	Capacity/ mAh g ⁻¹	Capacity retention (cycles)	Reference
------	--------------	----------------	----------------------------------	-----------------------------	-----------

Foil	LTO	1	155	-	[69]
		20	65	-	
Foil	Li/LFP	0.5	150	58% (300)	[89]
Foil	Li/NMC11	50 ^a	150	60% (300)	[90]
Foil	Li/LFP	2	110	33% (200)	[91]
Foil	Li/LFP	0.5	150	~100% (50)	[92]
Foil	Li/LFP	0.5	149	80% (100)	[94]
		5	15	-	
Foil	Si	-	800	85% (40)	[99]
Foil	Sn	100 ^a	300	75% (20)	[100]
Foil	Si	0.035 ^a	2428	53% (200)	[103]
Foil	Si	600 ^a	3250	50% (25)	[104]
Foil	Si	0.5	2021	10% (35)	[106]
Foil	C/LFP	1	955	96% (400)	[107]
		4	888	-	
Foil	LTO	0.1	151	-	[108]
		2	126	85% (200)	
		10	84	-	
Foil	Li/LFP	0.1	160	-	[109]
		0.5	150	57% (300)	
		5	120	-	
Foil	Li/LFP	0.2	115	-	[111]
		1	55	92% (200)	
		2	30	-	
Mesh	Li/ LTO	0.2	145	-	[85]
		4	85	80% (500)	
		10	60	-	
Foam	Li/LFP	0.5	150	90% (300)	[89]
Foam	Li/NMC11	50 ^a	150	90% (300)	[90]
Foam	Li/LFP	2	120	75% (200)	[91]
Foam	Li/LFP	0.5	151	~100% (50)	[92]
Foam	Li/LFP	0.5	149	90% (100)	[94]
		5	45	-	
Foam	Li/LFP	1	158	90% (200)	[96]
		10	124	-	

Foam	Graphite	0.2	285 (1.2 mm) ^b	-	[97]
			335 (0.6 mm) ^b	-	
			370 (0.3 mm) ^b	-	
Foam	Si	-	800	~100% (60)	[99]
Foam	Sn	100 ^a	850	59% (50)	[100]
Etched	Si	0.035 ^a	4255	80% (200)	[103]
Etched	Si	600 ^a	3250	74% (25)	[104]
Etched (wholely)	Si	0.5	2267	48% (100)	[106]
Etched (selectively)	Si	0.5	2758	71% (100)	[106]
Carbon- coated	LTO	1	160	-	[69]
		20	80	-	
Carbon- coated	C/LFP	1	996	97%(400)	[107]
		4	946	-	
Graphene- coated	LTO	0.1	155	-	[108]
		2	132	97% (200)	
		10	107	-	
CuO-coated	Li/LFP	0.1	160	-	[109]
		0.5	150	81% (300)	
		5	125	-	
Ag-coated	Li/LFP	0.2	125	-	[111]
		1	72	98% (200)	
		2	50	-	
Ni-coated	Li/LCO	0.2	120	-	[112]
		5	90	96% (250)	
		10	30	-	
ZnO-coated	Li/LCO	1	153	-	[113]
		10	99	84% (1000)	
		30	78	-	
β -PVDF- coated	Li/LFP	0.3	150	96% (40)	[114]
				47% (100)	

671 Note: When current collectors are tested in full cells, the 2nd column is expressed as
672 anode/cathode, as noted for other tables.

673 ^a denotes a different unit of mA g⁻¹ for current rate.

674 ^b denotes specific electrode thicknesses.

675 **3.3 Ni**

676 3.3.1 Electrochemical stability

677 Zhuang et al. performed a cyclic voltammetry study of Ni in 1.2 M LiPF₆ in EC:EMC
678 (3:7 vol.%) electrolyte, in a potential range from 0.5 – 2.9 V vs. Li/Li⁺, as shown in Fig.
679 4a [115]. A large cathodic peak can be seen at 1.85 V vs. Li/Li⁺ in the first cycle, which
680 is probably due to the reduction of Ni oxide to Ni and the formation of the SEI on the
681 Ni surface. A further shift of the potential in the cathodic direction probably results in
682 underpotential deposition of Li on the Ni surface. No alloying reaction was observed
683 as the potential moved close to 0 V vs. Li/Li⁺ [116]. The peaks in the anodic direction
684 were not well explained by the authors, which may arise from the dissolution of
685 deposited Li, oxidation of Ni and decomposition of the SEI. After the first cycle, the
686 overall current density remains below 5 μA cm⁻², indicating good electrochemical
687 stability in this potential range. Therefore, it is possible to use Ni as current collectors
688 for anodes.

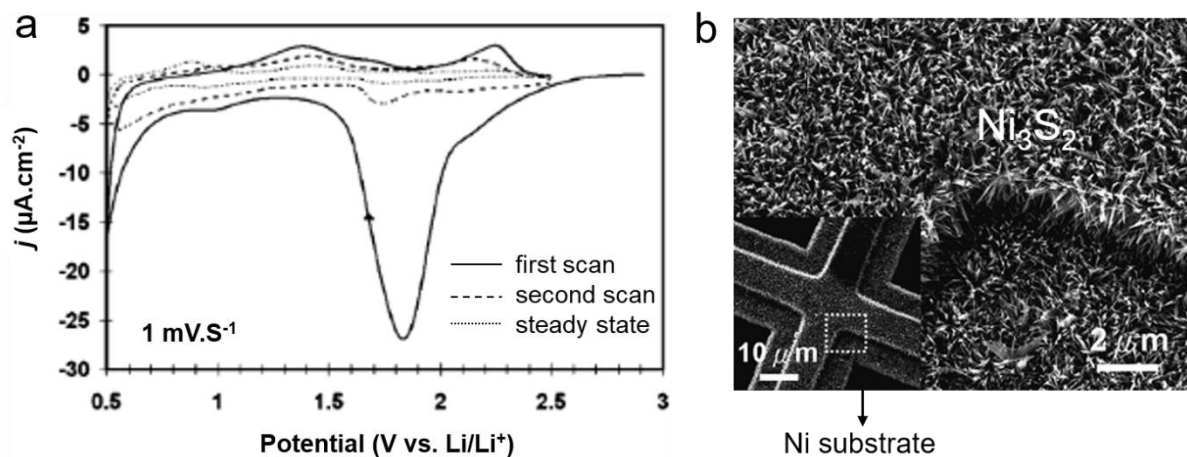
689 The electrochemical behaviour of Ni in the electrolytes of 1 M LiClO₄ in ethylene
690 carbonate (EC):diglyme (DG) (1:1 vol.%) and 1 M LiPF₆ in EC:DG (1:1 vol.%) in a high
691 potential range of 3 – 5.5 V vs Li/Li⁺ was investigated by Geoffroy et al. [117]. It was
692 reported that Ni was stable in the electrolytes up to 4.5 V vs Li/Li⁺. However, different
693 conclusions were drawn by other studies. Liu et al. reported that Ni corroded at a
694 potential of 3.6 V vs Li/Li⁺ in LiPF₆ in EC/DMC/DEC (1:1:1 vol.%) electrolyte [118].
695 Veith and Dudney proposed that Ni promoted the electrochemical degradation of
696 electrolytes containing LiPF₆ at potentials higher than 3.5 V vs Li/Li⁺ [119]. Overall, the
697 electrochemical behaviour of Ni current collectors has not been well studied,
698 particularly at high potentials, which hinders its application as current collectors for
699 cathodes.

700 3.3.2 Ni current collector

701 Ni foils have been used as current collectors for many anodes, e.g. Si [120, 121], SnO₂
702 [122], graphene [123], Sn/graphene composite [124], Co₃O₄ [125], NiO [126] and Ni₃S₂
703 [127], indicating a broad applicability. Compared with Cu foils, Ni foils have a very
704 similar density of 8.90 g/cm³ and a higher resistivity of 6.93 x 10⁻⁸ Ωm at 20 °C [56].
705 The tensile strength of 20 μm thick Ni foils made by electrodeposition is 730 MPa
706 [128], which is higher than that of Cu foils. The cost of Ni foils with a thickness of 20
707 μm and a purity of 99.9% is about \$ 795 /m², from the online quote of Goodfellow.

708 Ni current collectors have a unique advantage when used as current collectors for Ni
709 oxide and sulfide anodes, Ni can serve as not only the current collector but also a
710 source of the metal precursor. Varghese et al. fabricated vertically aligned NiO
711 nanowalls directly on a Ni foil using a plasma-assisted oxidation method [126]. The
712 as-fabricated NiO anode exhibits a reversible capacity of about 638 mAh g⁻¹ at a
713 current rate of 1.25 C after 85 cycles, which is close to the theoretical capacity of 718
714 mAh g⁻¹ [129]. Similarly, Lai et al. grew Ni₃S₂ nanowires directly on Ni substrates (Fig.
715 4b) [127]. The Ni₃S₂ anode delivers a reversible capacity of about 340 mAh g⁻¹ at 0.1
716 C after 100 cycles, which is about 65% of the theoretical capacity [130]. The direct
717 fabrication of Ni oxide and sulfide anodes on the Ni foils provides a good bonding
718 between anodes and current collectors and eliminates the need of using binders,
719 resulting in improved electrode performance.

720 Ni mesh [131, 132], foam [133-145] and etched Ni [146-148], have also been used as
721 current collectors for LIBs. Table 3 summarizes various Ni current collectors
722 developed for LIBs during the past two decades. Generally, the benefits from the mesh
723 and foam structures as well as surface modification for Ni current collectors are quite
724 similar to that for Al and Cu current collectors.



726 Fig. 4 a) Cyclic voltammogram of Ni electrode in 1.2 M LiPF₆ in EC:EMC (3:7 vol.%)
727 electrolyte (Reproduced with permission [115]. Copyright 2005 Elsevier), b) SEM
728 image of Ni₃S₂ nanoarrays grown on a Ni substrate (Reproduced with permission [127].
729 Copyright 2009 Royal Society of Chemistry).

730 **Table. 3 Ni current collectors**

Type	Electrode	Current rate/C	Capacity/ mAh g ⁻¹	Capacity retention (cycles)	Reference
Foil	Si	2	1700	59% (1250)	[120]
Foil	Si	1	3700	~100% (200)	[121]
		2	3500	~100% (200)	
Foil	SnO ₂	0.1	1121	58% (100)	[122]
		5	350	-	
Foil	Graphene	0.17	400	-	[123]
		2.67	280	-	
Foil	Sn and graphene composite	1	466	~100% (4000)	[124]
		2	300	-	
Foil	Co ₃ O ₄	1	1000	105% (20)	[125]
Foil	NiO	0.62	800	92% (40)	[126]
		1.25	638	97% (85)	
		1.86	500	~100% (50)	
Foil	Ni ₃ S ₂	0.1	400	80% (100)	[127]
Foil	Si (100 nm) ^a	1	2600	77% (400)	[147]
	Si (200 nm) ^a	1	1500	13% (500)	
Mesh	SnSb	60 ^b	500	60% (50)	[131]
Mesh	NiO	100 ^b	900	94% (20)	[132]
		10000 ^b	700	86% (20)	
Foam	C and Si composite	0.07	700	50% (95)	[133]
Foam	NiO	0.4	1.4 ^c	~100% (140)	[134]
Foam	NiO	0.5	844	85% (200)	[135]
		20	170	-	
Foam	NiO	156 ^b	701	92% (65)	[136]
		1310 ^b	200	-	
Foam	NiO	1000 ^b	706	95% (70)	[137]
		2000 ^b	548	80% (70)	
Foam	NiS	0.15	591	93% (100)	[138]
		5	394	-	
Foam	Ni ₃ S ₂	35 ^b	451	92% (80)	[139]
Foam	Si	0.2	2500	80% (100)	[140]
		4	803	-	

Foam	Si	0.025	2500	-	[141]
		0.5	1300	88% (100)	
		4	740	-	
Foam	ZnCo ₂ O ₄	500 ^b	1400	80% (50)	[142]
		1000 ^b	1300	72% (50)	
		2000 ^b	1100	49% (50)	
Foam	ZnCo ₂ O ₄	200 ^b	1986	-	[143]
		400 ^b	1900	130% (300)	
		5000 ^b	811	-	
Foam	ZnCo ₂ O ₄	100 ^b	1150	96% (60)	[144]
		416 ^b	1150	78%(50)	
Foam	Mn-doped Zn ₂ GeO ₄	100 ^b	1500	87% (100)	[145]
		2000 ^b	500	-	
Etched	Si	1	2400	75% (200)	[146]
Etched	Si	-	2650	66% (200)	[147]
Etched	Si (0.67 μm) ^a	1	2250	84% (200)	[148]
	Si (1.1 μm) ^a	1	2650	66% (200)	
	Si (1.8 μm) ^a	1	2800	39% (200)	
	Si (3.6 μm) ^a	1	1400	36% (60)	

731 ^a denotes specific electrode thicknesses.

732 ^b denotes a different unit of mA g⁻¹ for current rate.

733 ^c denotes a different unit of mAh cm⁻² for capacity.

734 3.4 Ti

735 3.4.1 Electrochemical stability

736 The electrochemical behaviour of Ti in 1 M LiPF₆ in EC:DMC (1:1 vol.%) electrolyte
737 was systematically investigated by Myung et al. (Fig. 5a) [30]. In the cathodic direction,
738 a small cathodic peak at 1.7 – 2.6 V vs Li/Li⁺ originates from the formation of the SEI
739 layer on the Ti surface. Further polarization results in the reduction of the air-formed
740 Ti oxide to Ti metal and underpotential deposition of Li on the Ti surface below 1.5V
741 vs. Li/Li⁺. Ti does not induce alloy formation with Li at low potentials close to 0. In the
742 anodic direction, an anodic peak at about 1.6 V vs Li/Li⁺ results from the oxidation of
743 the deposited Li and Ti metal. Similar to Al, further anodic polarization leads to the
744 formation of a passivation film which contains an outer layer of TiF₄ and an inner layer
745 of TiO₂ on the surface of the Ti metal (Fig. 5b), providing a relatively good corrosion

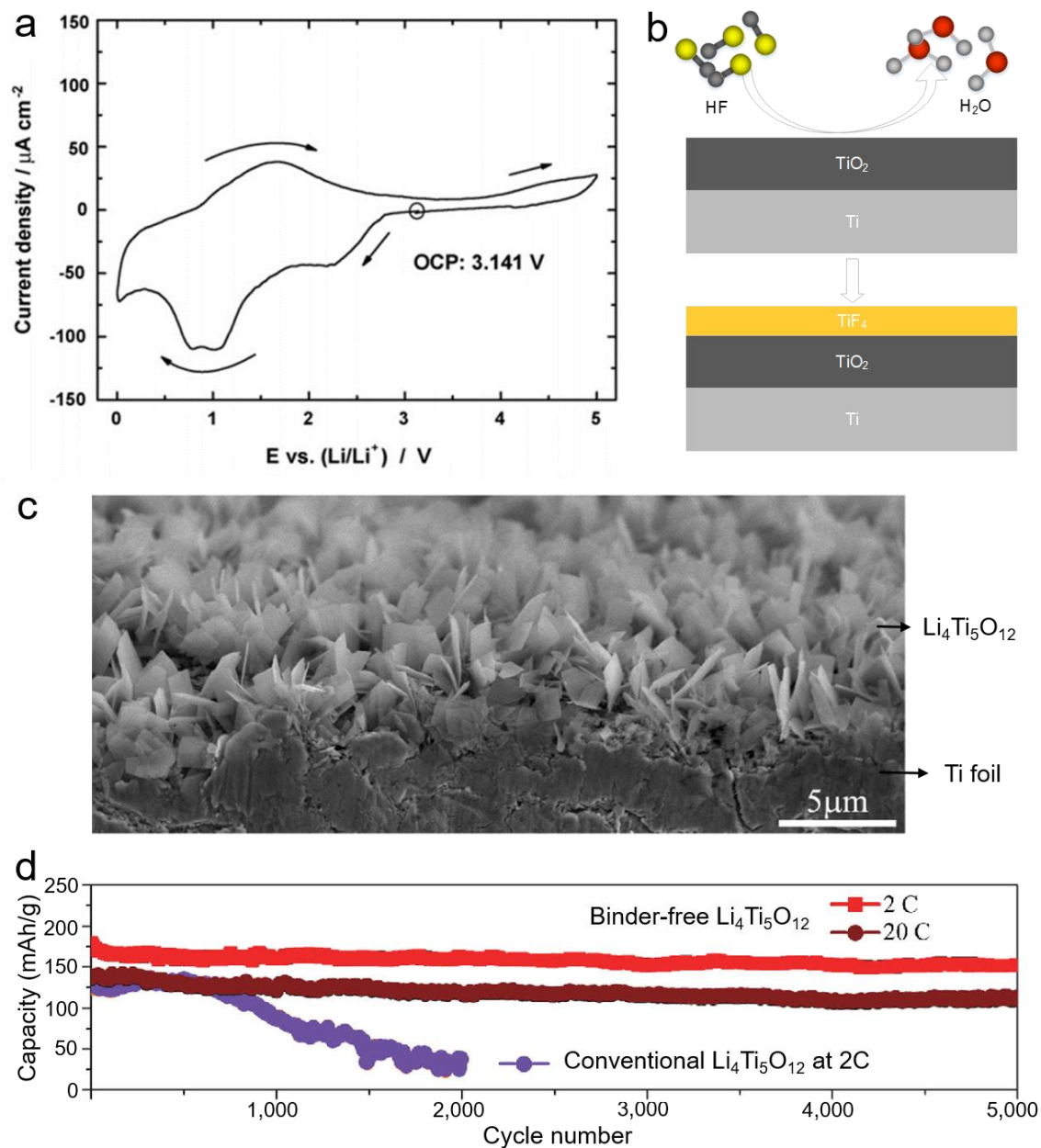
746 resistance at high potentials [76]. However, the passivation layer on the Ti surface
747 may not be as stable as that on the Al surface at high potentials, resulting in an inferior
748 performance when used as current collectors for cathodes [55]. Taken together, Ti is
749 stable in a wide potential range from 0 – 5 V vs Li/Li⁺ and can serve as current
750 collectors for both cathodes and anodes.

751 3.4.2 Ti current collector

752 Ti has a low density of 4.51 g/cm³ [56], lower than Cu and Ni but slightly higher than
753 Al. Ti foils with a thickness of 20 – 30 μm have a yield and tensile strength of 250 and
754 360 MPa [149], respectively, which is higher than Cu and Al. Adversely, Ti has a high
755 electrical resistivity of 3.9 x 10⁻⁷ Ωm at 20 °C [56], one order of magnitude higher than
756 the aforementioned metals. The cost of Ti foil with a thickness of 20 μm and a purity
757 of 99.9% is as high as about \$ 3100 /m², from the online quote of Goodfellow.

758 Ti foils have been used as current collectors for various electrodes, including CoO
759 [150], Co₃O₄ [151-154], SnO₂ [155, 156], Fe₂O₃ [157], TiO₂ [158, 159] and Li₄Ti₅O₁₂
760 [160, 161], as shown in Table 4. Ti can serve as a source of metal precursor when
761 used as current collectors for TiO₂ and Li₄Ti₅O₁₂ anodes. Besides, CoO, Co₃O₄, TiO₂
762 and Li₄Ti₅O₁₂ can directly grow on Ti surface without auxiliary binders and carbon black,
763 which is favourable to improving electrode capacity and cycle stability. A typical
764 example was done by Chen and his colleagues who fabricated Li₄Ti₅O₁₂ anodes on a
765 Ti foil current collector via a hydrothermal process without any additives [160]. The as-
766 fabricated Li₄Ti₅O₁₂ (Fig. 5c) exhibits a capacity of 124 mAh g⁻¹ at 50 C after 3000
767 cycles. Similar capacities of 153 and 115 mAh g⁻¹ at 2 C and 20 C after 5000 cycles,
768 respectively, were also reported for binder-free Li₄Ti₅O₁₂ anodes by Wang et al. [161].
769 For comparison, a conventional Li₄Ti₅O₁₂ anode with 20% carbon black and 10%
770 PVDF binder only delivers a capacity of 25 mAh g⁻¹ at 2 C after 2000 cycles (Fig. 5d).

771 Table 4 also summarizes Ti mesh and foam current collectors reported in the literature.
772 To our knowledge, etching and coating are not often employed to treat Ti current
773 collectors. The benefits from the mesh and foam structures for Ti current collectors
774 are quite similar to that for Al and Cu current collectors.



775

776 Fig. 5 a) Cyclic voltammety of Ti in 1 M LiPF₆ in EC:DMC (1:1 vol.%) electrolyte
 777 (Reproduced with permission [30]. Copyright 2009 Elsevier), b) schematic drawing of
 778 passivation film formed on Ti surface, c) Li₄Ti₅O₁₂ nanoarrays grown on Ti foil
 779 (Reproduced with permission [160]. Copyright 2014 Royal Society of Chemistry), d)
 780 Long-life cycling performance of binder-free and conventional Li₄Ti₅O₁₂ anodes
 781 (Reproduced with permission [161]. Copyright 2014 Springer Nature).

782 **Table. 4 Ti current collectors**

Type	Electrode	Current rate/C	Capacity/ mAh g ⁻¹	Capacity retention (cycles)	Reference	
Foil	CoO	1	700	96% (20)	[150]	
		2	500	93% (20)		
		4	375	83% (20)		
		6	200	75% (20)		
Foil	Co ₃ O ₄	20	600	75% (20)	[151]	
		50	400	60% (20)		
Foil	Co ₃ O ₄	1.5	750	~100% (30)	[152]	
		15	760	70% (30)		
		30	900	36% (30)		
Foil	Co ₃ O ₄	200 ^a	964	~100% (100)	[153]	
		5000 ^a	662	-		
Foil	Co ₃ O ₄ and α- Fe ₂ O ₃ composite	100 ^a	1200	82% (60)	[154]	
Foil		SnO ₂	0.2	980	71% (20)	[155]
			5	800	86% (20)	
Foil	SnO ₂	10	720	82% (20)	[156]	
		200 ^a	550	~100% (30)		
		1500 ^a	400	-		
Foil	α-Fe ₂ O ₃	200 ^a	893	-	[157]	
		500 ^a	814	112% (100)		
		10000 ^a	426	-		
Foil	TiO ₂	0.2	266	~100% (50)	[158]	
		10	66	-		
Foil	TiO ₂	0.05	340	-	[159]	
		2	125	-		
Foil	LTO	20	163	-	[160]	
		50	145	86% (3000)		
		200	78	-		
Foil	LTO	2	174	88% (5000)	[161]	
		20	139	83% (5000)		
		80	103	-		
Mesh	LMO	6.8	105	71% (1500)	[162]	
Mesh	TiO ₂	4.3 ^a	195	78% (100)	[163]	

Mesh	TiO ₂	10	267	-	[164]
		200	174	94% (6000)	
Mesh	LTO	1	188	-	[165]
		40	157	97% (325)	
		100	143	-	
Foam	TiO ₂	0.11	387	~100% (100)	[166]
		5.61	312	-	
Foam	TiO ₂	-	-	~100% (60)	[167]

783 ^a denotes a different unit of mA g⁻¹ for current rate.

784 3.5 Stainless steel

785 3.5.1 Electrochemical stability

786 Stainless steel is an alloy mainly containing Fe, Cr, Ni and Mn, which is well known for
787 high corrosion resistance due to the formation of a passivation film of chromium oxide
788 on the surface [168]. The electrochemical behaviour of stainless steel (type 304) in 1
789 M LiPF₆ in EC/DMC 1:1 electrolyte is shown in Fig. 6a [44]. A cathodic peak between
790 1.5 and 2 V vs. Li/Li⁺ is assumed to result from the reduction of the air-formed Fe-
791 and/or Cr-oxide films, the electrolytic salt formation of Li₂O, and the formation of the
792 SEI. Another cathodic peak occurs at about 0.6 V vs. Li/Li⁺, which is an indicator of
793 the underpotential deposition of Li on the stainless steel. No alloy between stainless
794 steel and Li is formed as the potential approaches 0 V vs. Li/Li⁺. In the anodic direction,
795 deposited Li starts to oxidize at 1 V vs. Li/Li⁺, generating an anodic peak current. As
796 the applied potential increases to 2 V vs. Li/Li⁺, another peak is observed due to the
797 oxidation of Cr. A small anodic peak occurs at about 3.2 V vs. Li/Li⁺, which is likely
798 due to the oxidation of Fe and Cr³⁺. Further increasing the applied potential up to 5 V
799 results in very small current, implying that a stable passivation film is formed.

800 However, The passivation film is not strong enough to protect stainless steel against
801 corrosion when used for LiCoO₂ and LiMn₂O₄ cathodes [169, 170]. Besides, the
802 electrochemical stability of stainless steel at high potentials is also affected by Li salts.
803 For example, stainless steel 304 is stable in 1 M LiPF₆ in EC/DEC electrolyte at
804 potentials up to 4.5 V vs. Li/Li⁺ but starts to react with the electrolyte of 1 M LiClO₄ in
805 EC/DEC at 3 V vs Li/Li⁺ [76]. Thus, the applicability of stainless steel current collectors
806 for cathodes is questionable. On the other hand, the stable electrochemical behaviour
807 at low potentials enables stainless steel to serve as current collectors for anodes.

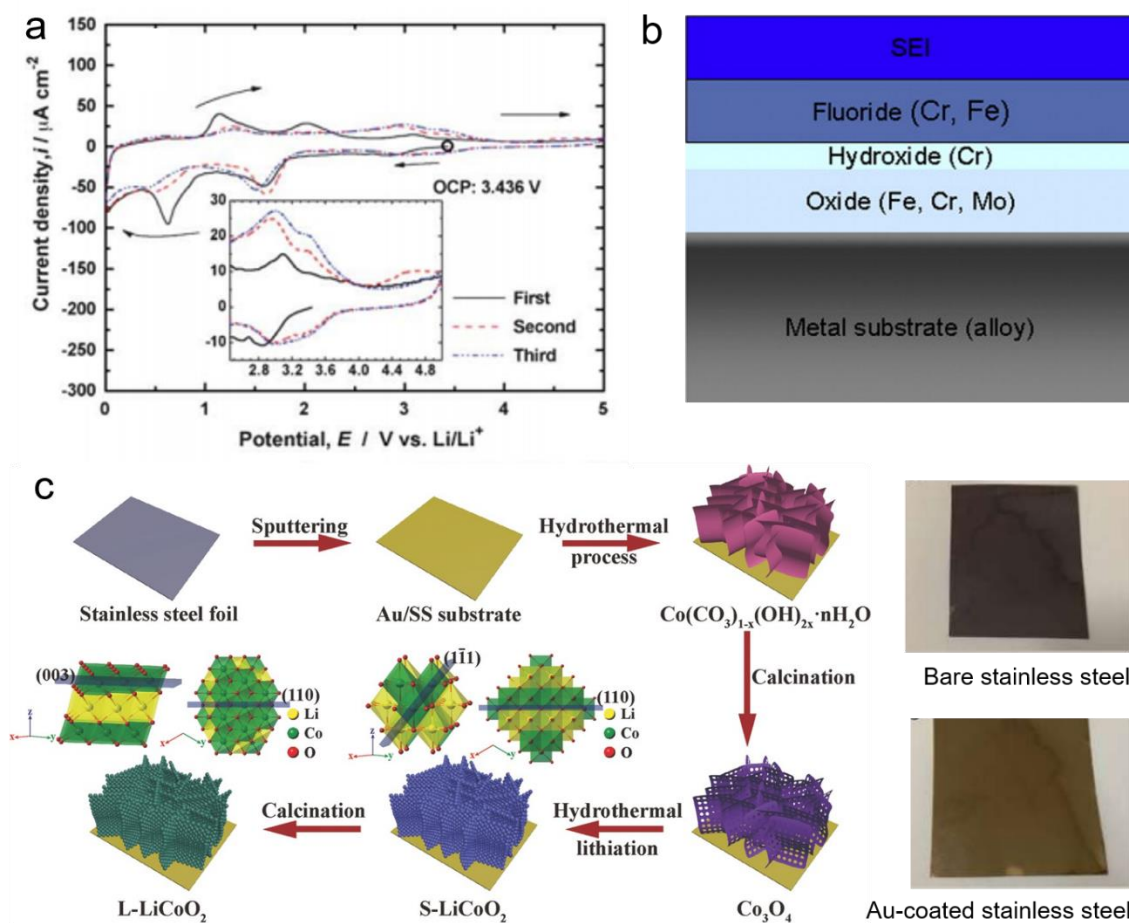
808 The electrochemical stability is also sensitive to the composition of stainless steel.
809 Fredriksson and Edström studied the electrochemical behaviour of duplex stainless
810 steel LDX 2101 in 1 M LiPF₆ in EC/DMC 1:1 electrolyte [171]. Stainless steel LDX
811 2101 is known to have a higher content of Cr and N as well as a lower content of Ni
812 than stainless steel 304, which results in stable electrochemical behaviour in a
813 potential range of 3 – 4.5 V vs Li/Li⁺. However, the stainless steel LDX 2101 is too
814 reactive with the EC/DMC electrolyte. Fredriksson and Edström also proposed a three-
815 layer structure of the passivation film on stainless steel LDX 2101, which is composed
816 of a bottom layer of iron and chromium oxides, an interlayer of chromium hydroxide
817 and a top layer of iron and chromium fluorides. The three-layer structure is also
818 expected to be applicable for stainless steel 304.

819 3.5.2 Stainless steel current collector

820 Stainless steel (type 304) has a density of 7.9 g/cm³, which is similar to Cu and Ni [48].
821 Stainless steel foils with a thickness of 25 μm have a tensile and yield strength of about
822 454 and 584 MPa [172], respectively, slightly higher than Cu foils. Adversely, stainless
823 steel has a high electrical resistivity of 7.2 x 10⁻⁷ Ωm at room temperature [48], which
824 is much higher than pure metals Cu, Al, Ni and Ti. The cost of stainless steel foils with
825 a thickness of 25 μm is about \$ 842 /m² (Goodfellow), which is similar to that of Cu
826 and Ni foils.

827 Stainless steel is superior to other metals when used as current collectors for Fe
828 contained anodes, e.g. α-Fe₂O₃ and FeVO₄. Li et al. directly fabricated α-Fe₂O₃
829 anodes on a stainless steel current collector via chemical corrosion in HCl and
830 subsequent thermal oxidation [173]. The as-fabricated α-Fe₂O₃ anode delivers a
831 capacity of 1105.6 mAh g⁻¹ at 0.2 C after 200 cycles, which is even higher than the
832 theoretical capacity, 1005 mAh g⁻¹. The stainless steel current collector serves as not
833 only mechanical support for α-Fe₂O₃ anodes but also a source of Fe³⁺. The direct
834 fabrication of α-Fe₂O₃ on the stainless steel current collector provides firm adhesion
835 and fast electron transport, avoiding the use of binder and carbon black. Similarly, Sim
836 et al. directly fabricated FeVO₄ anodes on a stainless steel foil via chemical vapour
837 deposition technique. The FeVO₄ anode exhibits a capacity of 1237 mAh g⁻¹ at 0.15 C
838 after 100 cycles, about 95% of the theoretical capacity [174].

839 Table 5 shows various stainless steel current collectors used for LIBs, including foil,
 840 mesh, coated and etched stainless steel. It is worth mentioning that all uncoated
 841 stainless steel current collectors are only used for anodes, which is indirect evidence
 842 that stainless steel may not be able to directly serve as a current collector for cathodes.
 843 With Au coating, stainless steel works perfectly for $\text{Li}(\text{Ni}_{0.5}\text{Mn}_{0.3}\text{Co}_{0.2})\text{O}_2$ and LiCoO_2
 844 cathodes [175, 176]. Fig. 6c illustrates the synthesis procedure of the LiCoO_2
 845 nanosheet arrays on an Au-coated stainless steel current collector. Apart from coating,
 846 a nitriding heat treatment was developed to treat stainless steel, which heats stainless
 847 steel at a temperature higher than $1200\text{ }^\circ\text{C}$ in a nitrogen atmosphere. The nitrided
 848 stainless steel is stable at a potential higher than 5 V vs Li/Li^+ [177]. Overall, though
 849 stainless steel has been used as current collectors for many electrodes, the analysis
 850 of the advantages and disadvantages of stainless steel current collectors is scarce in
 851 the literature.



852

853 Fig. 6 a) Cyclic voltammety of stainless steel (type 304) in 1 M LiPF_6 in EC:DMC (1:1
 854 vol.%) electrolyte (Reproduced with permission [44]. Copyright 2011 Royal Society of

855 Chemistry), b) schematic drawing of passivation film formed on the surface of stainless
 856 steel (Reproduced with permission [171]. Copyright 2012 Elsevier), c) schematic
 857 illustration of the synthesis procedure of LiCoO₂ nanosheet arrays on Au-coated
 858 stainless steel, the right part is macrographs of a bare and an Au-coated stainless
 859 steel foil (Reproduced with permission [176]. Copyright 2018 John Wiley & Sons).

860 **Table. 5 Stainless steel current collectors**

Type	Electrode	Current rate/C	Capacity/ mAh g ⁻¹	Capacity retention (cycles)	Reference
Foil	α -Fe ₂ O ₃	0.2	858	129% (200)	[173]
		1	681	134% (500)	
		5	520	-	
Foil	FeVO ₄	0.15	1316	94% (100)	[174]
		15	453	-	
Foil	Si	-	0.06 ^c	67% (70)	[178]
Foil	Si	0.2 ^a	0.55 ^c	-	[179]
Foil	Si	0.2	1600	72% (50)	[180]
Foil	Si	0.2	3800	84% (40)	[181]
		0.5	3600	86% (40)	
		1	3000	83% (40)	
Foil	SiO ₂	0.005 ^a	646	~100% (250)	[182]
Foil	SnO ₂ and α - Fe ₂ O ₃ composite	0.1 ^a	1195	80% (50)	[183]
		0.3 ^a	600	78% (50)	
Foil	CoFe ₂ O ₄	1	910	63% (100)	[184]
		2	900	59% (100)	
		4	810	56% (100)	
Foil	N-doped carbon	0.2	750	113% (150)	[185]
		2	415	-	
Foil	CoP	400 ^b	737	53% (900)	[186]
Foil	NiO	1	604	42% (100)	[187]
Foil	NiO and C composite	1	800	81% (100)	[187]
Foil	Co ₃ O ₄	700 ^b	1000	60% (100)	[188]

Foil	Graphene and Co ₃ O ₄ composite	700 ^b	1150	70% (100)	[188]
Foil	Co ₃ O ₄	0.5	1200	42% (50)	[189]
Foil	ZnO	1	635	63% (100)	[190]
Mesh	Graphene oxide	50 ^b	530	60% (20)	[191]
		100 ^b	435	78% (20)	
Mesh	Co ₃ O ₄	100 ^b	850	90% (80)	[192]
		800 ^b	625	-	
Mesh	Fe ₂ O ₃ and NiCo ₂ O ₄ composite	1000 ^b	650	90% (100)	[193]
Mesh	N-doped carbon	200 ^b	2058	-	[194]
		5000 ^b	313	-	
Au- coated	NMC532	0.5	125	89% (100)	[175]
Au- coated	LCO	0.1	130	82% (1000)	[176]
		10	105	-	
Au- coated	V ₂ O ₅	0.33	265	~100% (20)	[195]
Etched	MnO ₂	0.2	1300	107% (100)	[196]
		1	915	89% (95)	

861 ^a denotes a different unit of mA cm⁻² for current rate.

862 ^b denotes a different unit of mA g⁻¹ for current rate.

863 ^c denotes a different unit of mAh cm⁻² for capacity.

864 3.6 Carbonaceous material

865 3.6.1 Electrochemical stability

866 Fig. 7a shows the electrochemical behaviour of fully-, semi-, non-graphitic carbon
867 fibres and an Al foil in 1.2 M LiPF₆ in EC/DMC (1:2 vol.%) electrolyte [197]. The
868 passivation film on the Al foil is expected to form after the 1st cycle. Before 4.5 V vs
869 Li/Li⁺, the currents generated at all carbon fibres are close to that of the Al foil at the
870 2nd cycle, indicating that all carbon fibres have good electrochemical stability. The
871 current of all carbon fibres increases significantly after 4.5 V vs Li/Li⁺ due to oxidation.
872 It should be noted that the current in Fig. 7a is normalised by the geometric surface
873 area. Considering that the carbon fibres have much higher electroactive surface areas,
874 i.e. the surface area where chemical reactions take place, than the Al foil, the real
875 areal current densities on the carbon fibres should be much lower than that of the Al

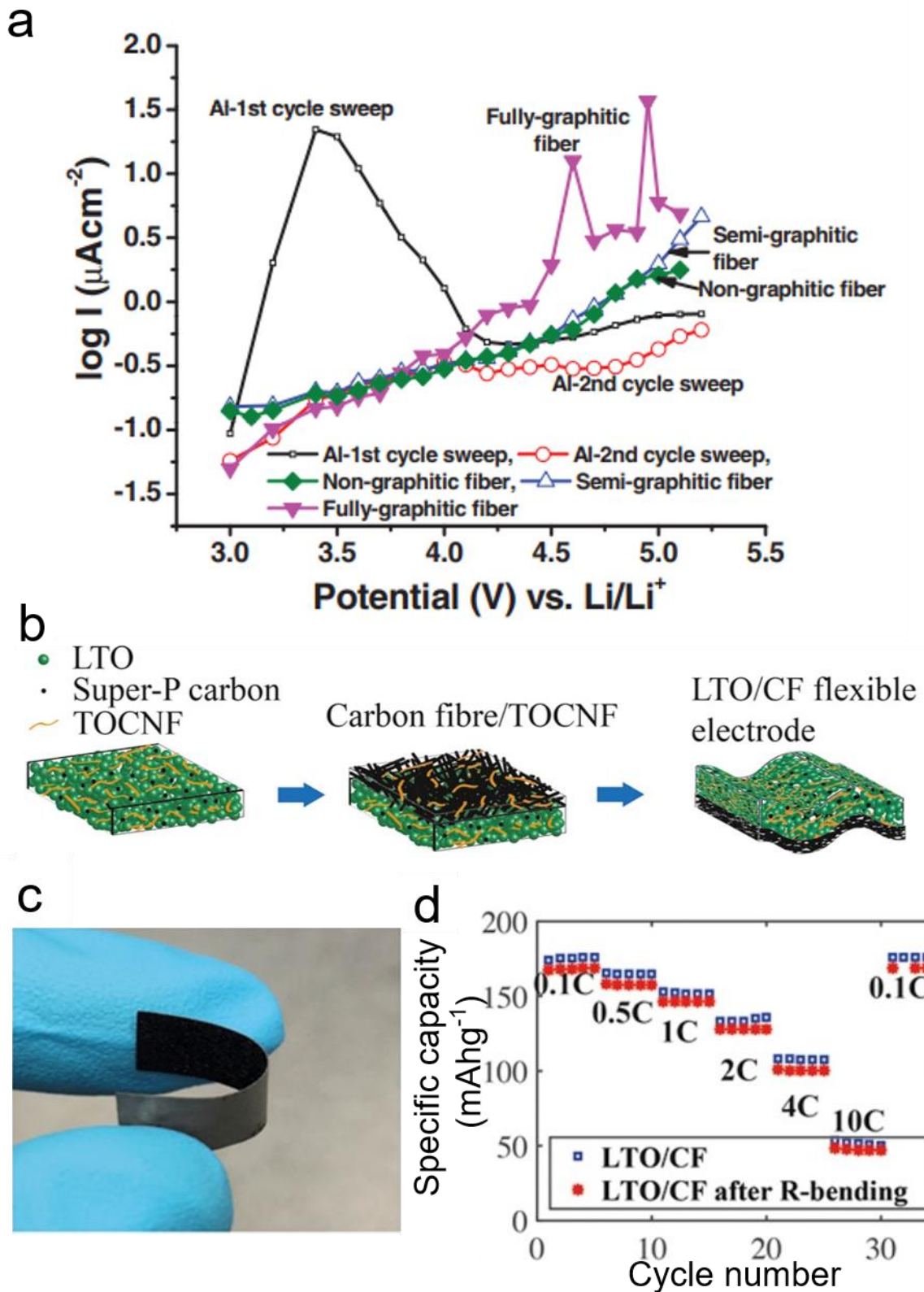
876 foil, indicating better electrochemical stability. Additionally, carbonaceous materials
877 have been widely used as conductive additives, e.g. carbon black, and even anodes,
878 e.g. graphite and graphene in LIBs [198], indicating good electrochemical stability at
879 a wide potential range. Thus, carbonaceous materials can serve as current collectors
880 for both cathodes and anodes.

881 3.6.2 Carbonaceous current collector

882 Carbonaceous current collectors, e.g. carbon fibre papers, are superior to metal
883 current collectors in many aspects. Firstly, carbonaceous current collectors are
884 favourable to increasing the ratio of active to non-active material at electrodes. Carbon
885 fibre papers with a porosity of 78% have a density of 0.44 g/cm³ [199], which is one
886 order of magnitude lower than that of metal foils. Besides, the porous structure allows
887 several times higher mass loading than planar metal current collectors and thus higher
888 gravimetric capacity [200, 201]. Secondly, carbonaceous substrates for anodes not
889 only serve as current collectors but also participate in lithiation/delithiation processes
890 as active materials, which further contribute to high battery capacity. Shafiei and Alpas
891 coated Sn anodes on a carbon fibre paper which serves as both a current collector
892 and active material [202]. The Sn-coated carbon fibre delivers an initial discharge
893 capacity of about 3 mAh cm⁻², almost four times higher than that of a Sn anode on a
894 Cu foil current collector. Thirdly, carbonaceous current collectors have unique
895 mechanical properties. The tensile strength of carbon fibre paper, with a mass fraction
896 of carbon fibre in the range of 0 – 50%, is up to 5 MPa [203]. Unlike metal current
897 collectors that easily undergo plastic deformation, carbonaceous current collectors
898 can be folded multiple times without plastic deformation, which is an ideal material for
899 future flexible LIBs [204]. Fig. 7b-d shows a flexible Li₄Ti₅O₁₂ anode on a carbon fibre
900 paper current collector, which delivers a capacity higher than 150 mAh g⁻¹ after
901 repeated bending [205]. A similar study for developing flexible current collectors based
902 on carbonaceous materials can be found in [206]. Fourthly, carbonaceous current
903 collectors can improve electron and ion transfer kinetics. Though carbon fibre papers
904 have a relatively high electrical resistance of 8 x 10⁻⁴ Ωm [199], the porous structures
905 of carbonaceous current collectors provide high contact area between electrodes and
906 current collectors as well as pathways for Li-ion diffusion, lowering interfacial
907 resistance and increasing mass transfer kinetics [207-210]. Additionally, the flexible
908 structure of carbonaceous materials can effectively alleviate strain and stress caused

909 by battery cycling, maintaining good current collector/electrode contact and thus high
910 conductivity. Last but not least, carbonaceous current collectors are cheaper than
911 metal current collectors. According to the online quotation from Goodfellow, carbon
912 fabric with a thickness of 0.15 mm costs \$ 440 /m², which is equivalent for \$ 60 /m² for
913 carbon fabric with a thickness of 20 μm.

914 In addition to carbon fibre papers, many other carbonaceous materials have also been
915 used as current collectors for LIBs; carbon foams, carbon nanotubes, carbon
916 nanofibres and graphene foams. Chu et al. fabricated carbon foams with an average
917 pore size of 39 nm and a BET surface area about 350 m²/g by the carbonization of
918 melamine foams at a high temperature of 800 °C and subsequent punching [211].
919 Nanosized TiO₂ anode was deposited on the as-fabricated carbon foam current
920 collectors, which exhibits a capacity of 203 and 104 mAh g⁻¹ at 0.3 and 6 C,
921 respectively. Carbon foam current collectors have also been fabricated by the
922 carbonization of melamine or PVDF for silicon anodes in other studies [212, 213]. A
923 10-layer carbon nanotube current collector with an extremely low density of 2 mg/cm³
924 has been fabricated for silicon anodes [214]. The silicon anode on the carbon
925 nanotube current collector delivers a high capacity of about 1600 mAh g⁻¹ at 100 mA
926 g⁻¹ and remains at 94% after 45 cycles. Besides this, the carbon nanotube current
927 collector has also been used in the development of flexible LIBs [215-217]. Kim
928 developed a 3D Si/carbon nanofibre anode by electrospinning [218]. Though the
929 authors described the anode as current collector-free, carbon nanofibres serve as a
930 mechanical support and current collector for silicon nanoparticles. The silicon anode
931 exhibited a high initial capacity of 1957 mAh g⁻¹ at 2 A g⁻¹ and maintained at about 60%
932 after 400 cycles. Carbon nanofibre current collectors with ultrafine titanium nitride
933 sheath decoration have also been used for Li metal anodes to alleviate the formation
934 of Li dendrites [219]. Chao and his colleagues directly fabricated V₂O₅ nanoarrays
935 cathode on a graphene foam (also named 'ultrathin graphite foam' in some
936 publications) via a solvothermal synthesis process [220]. The graphene foam has an
937 ultrahigh porosity of 99.7% and an electrical resistance of 10⁻³ Ωm which is similar to
938 carbon fibre papers, serving as a current collector. The V₂O₅ cathode on the graphene
939 foam delivers a capacity of 265 and 168 mAh g⁻¹ at 5 and 60 C, respectively. The
940 capacity remains at 98% at 60 C after 1000 cycles. Many other studies on graphene
941 foam current collectors have been reported in [221-223].



942

943 Fig. 7 a) Cyclic voltammetry of fully-, semi-, non-graphitic carbon fibres and Al foil in
 944 1.2 M LiPF₆ in EC/DMC (1:2 vol.%) electrolyte (Reproduced with permission [197].
 945 Copyright 2012 IOP Publishing), b) preparation of Li₄Ti₅O₁₂ anode on carbon fibre (CF)

946 current collector, with super-b carbon black and TEMPO oxidized cellulose nanofibrils
 947 (TOCNF) as a binder, c) macrograph of the flexible $\text{Li}_4\text{Ti}_5\text{O}_{12}$ anode on a carbon fibre
 948 current collector, d) capacity vs. cycle number measured at different rates of the
 949 $\text{Li}_4\text{Ti}_5\text{O}_{12}$ anode before and after repeat bending (R-bending) (Reproduced with
 950 permission [205]. Copyright 2017 Elsevier).

951 **Table. 6 Carbonaceous current collectors**

Type	Electrode(s)	Current rate/C	Capacity/ mAh g^{-1}	Capacity retention (cycles)	Reference
CFP	Si	0.1	1800	75% (40)	[200]
CFP	Si	0.1	700	93% (100)	[201]
CFP	Sn	1.5 ^a	152	50% (20)	[202]
CFP	LTO	0.1	166	-	[205]
		2	124	83% (100)	
		10	50	-	
CFP	LFP	0.1	150	-	[206]
		1	133	-	
CFP	Si and reduced graphene oxide composite	0.1	1100	-	[208]
		2.5	550	95% (100)	
		10	280	-	
CFP	Si	1	700	98% (10)	[209]
CFP	LVP and carbon composite	0.5	122	-	[210]
		10	108	95% (1000)	
		1	97.4	-	
CF	TiO_2	0.3	203	-	[211]
		3	150	75% (100)	
		6	104	-	
CF	Si	2000 ^b	1500	86% (1000)	[212]
CF	Si	0.05	2200	81% (123)	[213]
		0.1	2200	61% (142)	
		0.2	2040	69%(112)	
		50 ^b	1720	-	
CNT	Si	50 ^b	1720	-	[214]
		100 ^b	1590	94% (45)	

		800 ^b	100	-	
CNT	LTO	1	153	93% (200)	[215]
CNT	LTO	0.25	132	~100% (80)	[216]
CNT	LCO	0.25	134	93% (80)	[216]
CNT	LTO	10 ^b	160	94% (350)	[217]
CNF	Si	2000 ^b	1957	61% (400)	[218]
CNF	Li/LFP	1	160	78% (250)	[219]
GF	V ₂ O ₅	5	265	~100% (500)	[220]
		60	168	98% (1000)	
GF	Ge	1	1220	96%(1000)	[221]
		40	800	-	
GF	FeS ₂	0.2	1250	86% (100)	[222]
GF	Li/LFP	0.5	160	88% (100)	[223]
		2	106	-	

952 Note: CFP, CF, CNT, CNF and GF stands for carbon fibre paper, carbon foam,
 953 carbon nanotube, carbon nanofibre and graphene foam, respectively.

954 ^a denotes a different unit of mA cm⁻² for current rate.

955 ^b denotes a different unit of mA g⁻¹ for current rate.

956 4. Summary

957 4.1 Comparison of materials

958 Fig. 8a compares the performance of all materials reviewed in this work in five aspects.
 959 Carbon fibre paper is used to represent carbonaceous materials in comparison. In
 960 terms of electrochemical stability, Ti and carbon fibre have the largest stable potential
 961 range of 0 – 5 V vs. Li/Li⁺, allowing them to be employed as current collectors for both
 962 cathodes and anodes. Al has a relatively large stable potential range of ~0.5 – 5 V vs.
 963 Li/Li⁺ because the alloying reaction of Al and Li takes place at potentials close to 0 V
 964 vs. Li/Li⁺. Cu and Ni are stable at potentials up to 3.5 V vs. Li/Li⁺. Stainless steel has
 965 the smallest stable potential range of 0 – 3 V vs. Li/Li⁺. Thus, Cu, Ni and stainless steel
 966 can be used as current collectors for anodes only.

967 The second criterion is electrical conductivity. Cu has the lowest resistivity of 1.68 x
 968 10⁻⁸ Ωm, followed by Al (2.65 x 10⁻⁸ Ωm), Ni (6.93 x 10⁻⁸ Ωm), Ti (3.9 x 10⁻⁷ Ωm),
 969 stainless steel (7.2 x 10⁻⁷ Ωm) and carbon fibre paper (8 x 10⁻⁴ Ωm). A common query
 970 about the performance of Al current collectors is the effect of the air-formed Al₂O₃ layer

971 on the electrical conductivity. Comparing the theoretical electrical conductivity of pure
972 Al and the measured electrical conductivity of untreated Al wires and rods shows that
973 the Al_2O_3 layer does not affect the electrical conductivity of Al current collectors. It is
974 generally accepted that other metals and carbon-based materials are stable under the
975 exposure of air. To the best of our knowledge, very little work has been done on the
976 effect of passivation films on the electrical conductivity of current collectors. The
977 contact resistance between the current collector and electrode is much higher than the
978 resistance of the current collector itself and there has been much work in modifying
979 the surface to improve adhesion and through-plane conductivity. It is necessary to
980 minimise the contact resistance to improve the overall conductivity in practical
981 applications.

982 In terms of tensile strength, the order of the metal foils from high to low, is Ni (730
983 MPa), stainless steel (454 MPa), Ti (360 MPa), Cu (~325 MPa) and Al (25 MPa).
984 Carbon fibre papers have a tensile strength lower than 5 MPa. Advantageously, the
985 soft structure makes carbon fibre paper an ideal choice for flexible current collectors.

986 When it comes to density, carbon fibre papers are the lightest material with a density
987 of about 0.44 g/cm^3 , followed by Al (2.7 g/cm^3), Ti (4.51 g/cm^3), stainless steel (7.9
988 g/cm^3), Ni (8.9 g/cm^3) and Cu (8.96 g/cm^3). As the conventional Cu current collector
989 takes up 13% of the total weight of a LIB, assuming other conditions are the same,
990 replacing the Cu foil with an identically sized carbon fibre paper as the current collector
991 is expected to reduce the total weight of the LIB by 12% and thus increase the
992 gravimetric capacity by 14%.

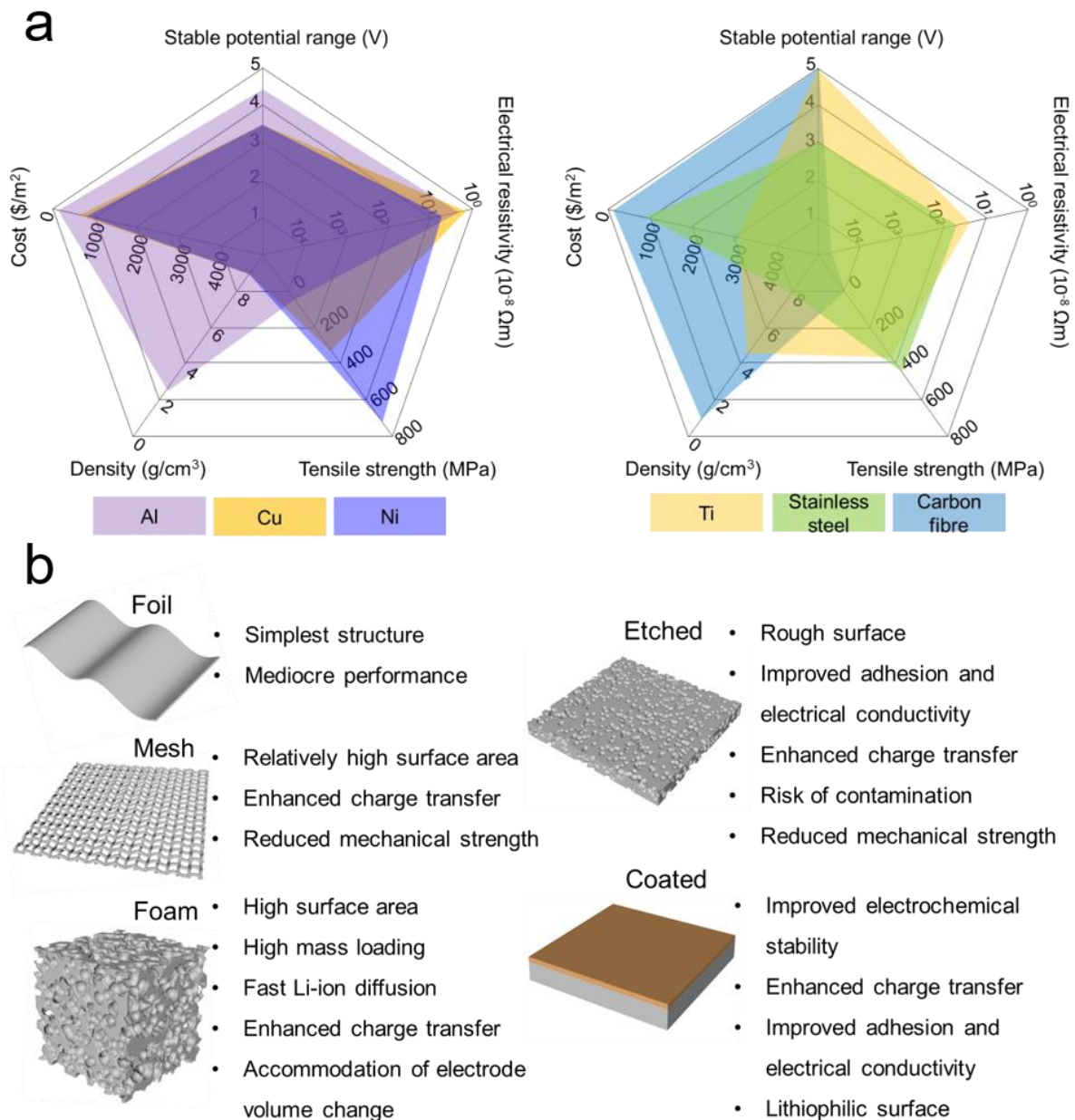
993 Last but not least, the cost and sustainability vary with materials greatly. Based on the
994 online quotation from Goodfellow in June 2020, the order of the six types of foils in
995 cost, from low to high, is carbon fabric ($\$ 60 /\text{m}^2$), Al ($\$ 130 /\text{m}^2$), Cu ($\$ 640 /\text{m}^2$), Ni
996 ($\$ 795 /\text{m}^2$), stainless steel ($\$ 842 /\text{m}^2$) and Ti ($\$ 3100 /\text{m}^2$). All of the foils have similar
997 thicknesses around $20 \mu\text{m}$ and purity higher than 99%. In terms of sustainability,
998 carbon is the most abundant material among the six materials, followed by Al, stainless
999 steel (based on Fe reserve), Ti, Ni and Cu [224, 225]. Recyclability is an important part
1000 of sustainability. It is reported that Al and Cu foils can be easily separated from
1001 electrode active materials by ultrasonic treatments or heating and then recycled or

1002 reused [226-228]. However, the recyclability of other materials has not been well
1003 investigated.

1004 **4.2 Effects of structures and treatments**

1005 Current collectors are normally employed in the forms of foil, mesh and foam. Foil is
1006 the simplest structure which is easy to produce and process. However, the mediocre
1007 performance of foil current collectors makes it is difficult to meet the requirements for
1008 next-generation LIBs. Mesh current collectors are expected to improve electrode
1009 performance due to increased surface area and enhanced charge transfer kinetics.
1010 The limitation is that mesh current collectors have low mechanical strength. Foam
1011 current collectors can provide even higher surface area than mesh current collectors.
1012 Besides, the porous structure also allows high mass loading, efficient Li-ion diffusion,
1013 fast charge transfer and accommodation of electrode volume change during cycling,
1014 greatly improving electrode performance. It also should be noted that the electrode
1015 loading technique is crucial when using mesh and foam current collectors. For
1016 example, a large amount of active material can be loaded evenly on foam current
1017 collectors by electrodeposition, thus enhancing performance, while very limited active
1018 material can be loaded via dip-coating, causing a huge waste of useful surface area.

1019 Chemical etching and coating are two commonly used treatments for current collectors.
1020 Chemical etching can effectively roughen the surface of current collectors, which is
1021 favourable for improving adhesion and interfacial conductivity between electrodes and
1022 current collectors as well as electrode/electrolyte charge transfer kinetics. Current
1023 collectors with patterns for particular purposes can be fabricated by selective etching
1024 to alleviate the volume change of some specific anodes. Nevertheless, chemical
1025 etching may also bring a risk of contamination and reduce the mechanical strength of
1026 current collectors. Coating is an effective way to change the surface material to
1027 achieve better performance. The coated material can improve the electrochemical
1028 stability, charge transfer property, interfacial adhesion and conductivity of current
1029 collectors. Besides, current collectors coated with lithiophilic materials, e.g. CuO and
1030 Ag, can reduce the nucleation overpotential and guide uniform Li nucleation and
1031 deposition, effectively preventing the formation of Li dendrites.



1032

1033 Fig. 8 a) Comparison of Al, Cu, Ni, Ti, stainless steel and carbon fibre in five aspects
 1034 of stable potential range, electrical resistivity, tensile strength, density and cost; b)
 1035 main advantages and disadvantages of current collectors with three different
 1036 structures of foil, mesh and foam, as well as two treatments of chemical etching and
 1037 coating. Note: the carbon fabric with a thickness of 0.15 mm costs \$ 440 /m², which is
 1038 equivalent for \$ 60 /m² for carbon fabric with a thickness of 20 μm.

1039 **4.3 Future directions**

1040 The development of next-generation LIBs will go in the direction of higher capacity,
 1041 longer service lifetime, more environmental-friendliness and lower cost, which requires

1042 potential current collectors to be more electrochemically stable, more conductive,
1043 lighter and cheaper. Additionally, current collectors with flexible structures are also
1044 necessary for the applications of future wearable devices. To achieve this goal, further
1045 efforts should be made on the following topics.

- 1046 • Carbonaceous materials have been regarded as a promising alternative to
1047 conventional Al and Cu current collectors in the literature. However, the use of
1048 carbonaceous materials in real LIBs is still problematic due to low weldability. At
1049 present, all metallic current collectors are connected with electrode tabs by welding,
1050 providing a good bonding and electrical contact. However, It is very hard to weld
1051 carbonaceous materials due to the extremely high temperature and pressure
1052 needed for melting [229]. Therefore, more efforts should be made on securing good
1053 contacts between the carbonaceous current collectors and electrode tabs.
- 1054 • Porous current collectors are ideal choices for high electrode mass loading [230,
1055 231]. On the one hand, the enhanced mass loading can improve absolute LIB
1056 capacity. On the other hand, the enhanced mass loading may sacrifice gravimetric
1057 capacity due to increased internal electrical resistance and limited Li-ion diffusion
1058 [98]. We need to optimise the porous structure of current collectors, e.g. porosity,
1059 pore size and pore shape, to increase electrode mass loading as well as keep
1060 electrical resistance low and Li-ion diffusion rate high. So we can improve both
1061 absolute and gravimetric capacity of LIBs at the same time.
- 1062 • Polymers have lower densities than metals and better mechanical strength than
1063 carbonaceous material, which is a potential material for current collectors [232]. In
1064 addition, polymers are expected to have better corrosion resistance than
1065 conventional metal current collectors. Nevertheless, low electrical conductivity is a
1066 major obstacle for polymeric current collectors. The electrical conductivity of
1067 polymeric current collectors needs further improvement to meet the requirements
1068 for high power LIBs. Another concern is the thermal conductivity and stability.
1069 Metallic current collectors transfer heat in addition to electrons. Future polymeric
1070 current collectors need similar high thermal conductivities to avoid heat
1071 accumulation in LIBs and provide thermal stability in the normal operating
1072 temperature range.
- 1073 • Surface coating is a commonly used treatment to make current collectors more
1074 stable, conductive and improve adhesion properties. Thick coatings can add extra

1075 weight to LIBs, while thin coatings may result in insufficient protection and
1076 conduction [70]. A uniform coating layer with an appropriate thickness is beneficial
1077 for high LIB performance. Thus, the coating thickness and uniformity need to be
1078 precisely controlled. Besides, the coating material is also an important factor.
1079 Current collectors coated with lighter and more conductive materials are desirable
1080 for the next generation LIBs.

1081 • Recycling or reusing conventional current collectors can not only protect our
1082 environment but also provide a secondary source of some valuable materials,
1083 reducing the cost of current collectors [29]. To our knowledge, although the
1084 strategy for the recycling of Al and Cu foils from end-of-life LIBs has been proposed
1085 in many studies [226-228], subsequent characterisation and testing of the recycled
1086 Al and Cu foils have not been well reported. Whether the recycled Al and Cu current
1087 collectors can be directly reused in new LIBs is still unknown. Furthermore,
1088 knowledge about the recyclability of other current collectors is still lacking and
1089 needs investigating.

1090 **Abbreviation**

CMC	Carboxymethyl cellulose
DG	Diglyme
EC	Ethylene carbonate
EMC	Ethyl methyl carbonate
DEC	Diethyl carbonate
DMC	Dimethyl carbonate
LCO	Lithium cobalt oxide, LiCoO_2
LFP	Lithium iron phosphate, LiFePO_4
LMO	Lithium manganese oxide, LiMn_2O_4
LNMO	Lithium nickel manganese oxide, $\text{LiNi}_{0.5}\text{Mn}_{1.5}\text{O}_4$
NMC	Lithium nickel manganese cobalt oxide, LiNiMnCoO_2
LTO	Lithium titanate oxide, $\text{Li}_4\text{Ti}_5\text{O}_{12}$
LVP	Lithium vanadium phosphate, $\text{Li}_3\text{V}_2(\text{PO}_4)_3$
MFA	Methyl difluoroacetate
PC	Propylene carbonate
β -PVDF	β -phase polyvinylidene difluoride

1091

1092 **CRedit authorship contribution statement**

1093 **Pengcheng Zhu:** Conceptualization, Investigation, Writing - original draft

1094 preparation, **Emma Kendrick** and **Vannessa Goodshipa:** Conceptualization,

1095 Funding acquisition, Project administration, **Dominika Gastol, Jean Marshall** and
1096 **Roberto Sommerville**: Investigation, Writing - Review & Editing.

1097 **Declaration of competing interest**

1098 The authors declare that they have no known competing financial interests or
1099 personal relationships that could have appeared to influence the work reported in
1100 this paper.

1101 **Funding**

1102 This research was funded by the Faraday Institution; ReLiB fast-start project (grant
1103 numbers FIRG005 and FIRG006), the Innovate UK through the Faraday Challenge;
1104 R2LIB, TS/S004572/1.

1105 **Reference**

- 1106 [1] J.-M. Tarascon, M. Armand, *nature*, 414 (2001) 359-367.
1107 [2] J.B. Goodenough, Y. Kim, *Chemistry of materials*, 22 (2010) 587-603.
1108 [3] L. Lu, X. Han, J. Li, J. Hua, M. Ouyang, *Journal of power sources*, 226 (2013) 272-288.
1109 [4] S. Pacala, R. Socolow, *science*, 305 (2004) 968-972.
1110 [5] I. Rubio Lopez, M.J. Lain, E. Kendrick, *Batteries & Supercaps*, (2020).
1111 [6] A. Jaiswal, *Renewable and Sustainable Energy Reviews*, 72 (2017) 922-934.
1112 [7] S.B. Chikkannanavar, D.M. Bernardi, L. Liu, *Journal of Power Sources*, 248 (2014) 91-100.
1113 [8] S. Goriparti, E. Miele, F. De Angelis, E. Di Fabrizio, R.P. Zaccaria, C. Capiglia, *Journal of power*
1114 *sources*, 257 (2014) 421-443.
1115 [9] C.-H. Chen, F.B. Planella, K. O'Regan, D. Gastol, W.D. Widanage, E. Kendrick, *Journal of The*
1116 *Electrochemical Society*, 167 (2020) 080534.
1117 [10] M. Marcinek, J. Syzdek, M. Marczewski, M. Piszcz, L. Niedzicki, M. Kalita, A. Plewa-Marczewska,
1118 A. Bitner, P. Wiczorek, T. Trzeciak, *Solid State Ionics*, 276 (2015) 107-126.
1119 [11] X. Huang, *Journal of Solid State Electrochemistry*, 15 (2011) 649-662.
1120 [12] J.T. Warner, *The handbook of lithium-ion battery pack design: chemistry, components, types and*
1121 *terminology*, Elsevier, 2015.
1122 [13] B.A. Johnson, R.E. White, *Journal of power sources*, 70 (1998) 48-54.
1123 [14] L.-P. He, S.-Y. Sun, X.-F. Song, J.-G. Yu, *Waste management*, 46 (2015) 523-528.
1124 [15] C.C. Wang, Y.C. Lin, K.F. Chiu, H.J. Leu, T.H. Ko, *ChemistrySelect*, 2 (2017) 4419-4427.
1125 [16] M.J. Lain, J. Brandon, E. Kendrick, *Batteries*, 5 (2019) 64.
1126 [17] S. Jin, Y. Jiang, H. Ji, Y. Yu, *Advanced Materials*, 30 (2018) 1802014.
1127 [18] M. Yamada, T. Watanabe, T. Gunji, J. Wu, F. Matsumoto, *Electrochem*, 1 (2020) 124-159.
1128 [19] M. Li, J. Lu, Z. Chen, K. Amine, *Advanced Materials*, 30 (2018) 1800561.
1129 [20] S. Murashige, N. Arai, in, *Google Patents*, 2004.
1130 [21] J.B. Goodenough, *Accounts of chemical research*, 46 (2013) 1053-1061.
1131 [22] C. Liu, Z.G. Neale, G. Cao, *Materials Today*, 19 (2016) 109-123.
1132 [23] S.J. An, J. Li, C. Daniel, D. Mohanty, S. Nagpure, D.L. Wood III, *Carbon*, 105 (2016) 52-76.
1133 [24] S. Zhang, T. Jow, *Journal of Power Sources*, 109 (2002) 458-464.

1134 [25] P.S. Kumar, S. Ayyasamy, E.S. Tok, S. Adams, M. Reddy, ACS omega, 3 (2018) 3036-3044.

1135 [26] A. Kraytsberg, Y. Ein - Eli, Advanced Energy Materials, 6 (2016) 1600655.

1136 [27] D. Ma, Z. Cao, A. Hu, Nano-Micro Letters, 6 (2014) 347-358.

1137 [28] J. Li, Z. Du, R.E. Ruther, S.J. An, L.A. David, K. Hays, M. Wood, N.D. Phillip, Y. Sheng, C. Mao, Jom, 69 (2017) 1484-1496.

1139 [29] G. Harper, R. Sommerville, E. Kendrick, L. Driscoll, P. Slater, R. Stolkin, A. Walton, P. Christensen, O. Heidrich, S. Lambert, Nature, 575 (2019) 75-86.

1141 [30] S.-T. Myung, Y. Sasaki, S. Sakurada, Y.-K. Sun, H. Yashiro, Electrochimica Acta, 55 (2009) 288-297.

1142 [31] K. Kanamura, T. Okagawa, Z.-i. Takehara, Journal of power sources, 57 (1995) 119-123.

1143 [32] X. Zhang, T. Devine, Journal of The Electrochemical Society, 153 (2006) B344-B351.

1144 [33] X. Zhang, T. Devine, Journal of The Electrochemical Society, 153 (2006) B375-B383.

1145 [34] J.W. Braithwaite, A. Gonzales, G. Nagasubramanian, S.J. Lucero, D.E. Peebles, J.A. Ohlhausen, W.R. Cieslak, Journal of the electrochemical society, 146 (1999) 448.

1147 [35] S. Wiemers-Meyer, S. Jeremias, M. Winter, S. Nowak, Electrochimica Acta, 222 (2016) 1267-1271.

1148 [36] X. Zhang, T.M. Devine, Journal of The Electrochemical Society, 153 (2006) B365-B369.

1149 [37] H. Yang, K. Kwon, T.M. Devine, J.W. Evans, Journal of The Electrochemical Society, 147 (2000) 4399-4407.

1151 [38] M. Morita, T. Shibata, N. Yoshimoto, M. Ishikawa, Electrochimica Acta, 47 (2002) 2787-2793.

1152 [39] X. Chen, W. Xu, M.H. Engelhard, J. Zheng, Y. Zhang, F. Ding, J. Qian, J.-G. Zhang, Journal of Materials Chemistry A, 2 (2014) 2346-2352.

1153 [40] K. Park, S. Yu, C. Lee, H. Lee, Journal of Power Sources, 296 (2015) 197-203.

1154 [41] S. Theivaprakasam, G. Girard, P. Howlett, M. Forsyth, S. Mitra, D. MacFarlane, NPJ Materials Degradation, 2 (2018) 1-9.

1157 [42] L. Zhang, L. Chai, L. Zhang, M. Shen, X. Zhang, V.S. Battaglia, T. Stephenson, H. Zheng, Electrochimica Acta, 127 (2014) 39-44.

1158 [43] S.-W. Song, T.J. Richardson, G.V. Zhuang, T.M. Devine, J.W. Evans, Electrochimica acta, 49 (2004) 1483-1490.

1161 [44] S.-T. Myung, Y. Hitoshi, Y.-K. Sun, Journal of Materials Chemistry, 21 (2011) 9891-9911.

1162 [45] T. Kawamura, T. Tanaka, M. Egashira, I. Watanabe, S. Okada, J.-i. Yamaki, Electrochemical and Solid-State Letters, 8 (2005) A459-A463.

1164 [46] G. Xu, P. Han, S. Dong, H. Liu, G. Cui, L. Chen, Coordination Chemistry Reviews, 343 (2017) 139-184.

1166 [47] A. Yoshino, K. Sanechika, T. Nakajima, in, Google Patents, 1987.

1167 [48] W. Haynes, C. Handbook, in, CRC Press, 2016.

1168 [49] L. Tian, A. Russell, T. Riedemann, S. Mueller, I. Anderson, Materials Science and Engineering: A, 690 (2017) 348-354.

1170 [50] R. Brandt, G. Neuer, International Journal of Thermophysics, 28 (2007) 1429-1446.

1171 [51] P.A. Nelson, K.G. Gallagher, I.D. Bloom, D.W. Dees, in, Argonne National Lab.(ANL), Argonne, IL (United States), 2012.

1173 [52] M. Lederer, V. Gröger, G. Khatibi, B. Weiss, Materials Science and Engineering: A, 527 (2010) 590-599.

1174 [53] P. Arora, M. Doyle, A.S. Gozdz, R.E. White, J. Newman, Journal of power Sources, 88 (2000) 219-231.

1175 [54] R.A. Hikmet, Journal of power sources, 92 (2001) 212-220.

1177 [55] K. Kanamura, W. Hoshikawa, T. Umegaki, Journal of the Electrochemical Society, 149 (2002) A339-A345.

1178 [56] S. Venkatraman, V. Subramanian, S.G. Kumar, N. Renganathan, N. Muniyandi, Electrochemistry communications, 2 (2000) 18-22.

1181 [57] X. Wang, H. Hao, J. Liu, T. Huang, A. Yu, Electrochimica acta, 56 (2011) 4065-4069.

1182 [58] S. Ramesh, K. Ramesh, A. Arof, Int J Electrochem Sci, 8 (2013) 8348-8355.

1183

1184 [59] M. Herklotz, F. Scheiba, R. Glaum, E. Mosymow, S. Oswald, J. Eckert, H. Ehrenberg, *Electrochimica*
1185 *Acta*, 139 (2014) 356-364.

1186 [60] M. Fritsch, G. Standke, C. Heubner, U. Langklotz, A. Michaelis, *Journal of Energy Storage*, 16 (2018)
1187 125-132.

1188 [61] K.G. Gallagher, S.E. Trask, C. Bauer, T. Woehrle, S.F. Lux, M. Tschech, P. Lamp, B.J. Polzin, S. Ha, B.
1189 Long, *Journal of The Electrochemical Society*, 163 (2016) A138-A149.

1190 [62] H. Zheng, J. Li, X. Song, G. Liu, V.S. Battaglia, *Electrochimica Acta*, 71 (2012) 258-265.

1191 [63] X. Du, Q. Wang, T. Feng, X. Chen, L. Li, L. Li, X. Meng, L. Xiong, X. Sun, L. Lu, *Scientific reports*, 6
1192 (2016) 20138.

1193 [64] T. Nakamura, S. Okano, N. Yaguma, Y. Morinaga, H. Takahara, Y. Yamada, *Journal of power*
1194 *sources*, 244 (2013) 532-537.

1195 [65] S. Yoon, H.-S. Jang, S. Kim, J. Kim, K.Y. Cho, *Journal of Electroanalytical Chemistry*, 797 (2017) 37-
1196 41.

1197 [66] S. Nakanishi, T. Suzuki, C. Qi, J. Akikusa, K. Nakamura, *Transactions of Nonferrous Metals Society*
1198 *of China*, 24 (2014) 2314-2319.

1199 [67] D.-Y. Shin, D.-H. Park, H.-J. Ahn, *Applied Surface Science*, 475 (2019) 519-523.

1200 [68] K. Striebel, J. Shim, A. Sierra, H. Yang, X. Song, R. Kostecky, K. McCarthy, *Journal of Power Sources*,
1201 146 (2005) 33-38.

1202 [69] H.-C. Wu, E. Lee, N.-L. Wu, T.R. Jow, *Journal of power sources*, 197 (2012) 301-304.

1203 [70] I. Doberdò, N. Löffler, N. Laszczynski, D. Cericola, N. Penazzi, S. Bodoardo, G.-T. Kim, S. Passerini,
1204 *Journal of power sources*, 248 (2014) 1000-1006.

1205 [71] S.R. Prabakar, Y.-H. Hwang, E.G. Bae, D.K. Lee, M. Pyo, *Carbon*, 52 (2013) 128-136.

1206 [72] S. Kang, H. Xie, W. Zhai, Z. Ma, R. Wang, W. Zhang, *Int. J. Electrochem. Sci*, 10 (2015) 2324-2335.

1207 [73] S. Gheytni, Y. Liang, Y. Jing, J.Q. Xu, Y. Yao, *Journal of Materials Chemistry A*, 4 (2016) 395-399.

1208 [74] S.Y. Kim, Y.I. Song, J.-H. Wee, C.H. Kim, B.W. Ahn, J.W. Lee, S.J. Shu, M. Terrones, Y.A. Kim, C.-M.
1209 Yang, *Carbon*, 153 (2019) 495-503.

1210 [75] H. Lee, J.-J. Cho, J. Kim, H.-J. Kim, *Journal of the Electrochemical Society*, 152 (2005) A1193-A1198.

1211 [76] C. Iwakura, Y. Fukumoto, H. Inoue, S. Ohashi, S. Kobayashi, H. Tada, M. Abe, *Journal of power*
1212 *sources*, 68 (1997) 301-303.

1213 [77] J. Kawakita, K. Kobayashi, *Journal of power sources*, 101 (2001) 47-52.

1214 [78] M. Zhao, S. Kariuki, H.D. Dewald, F.R. Lemke, R.J. Staniewicz, E.J. Plichta, R.A. Marsh, *Journal of*
1215 *the Electrochemical Society*, 147 (2000) 2874-2879.

1216 [79] S. Dai, J. Chen, Y. Ren, Z. Liu, J. Chen, C. Li, X. Zhang, X. Zhang, T. Zeng, *Int. J. Electrochem. Sci*, 12
1217 (2017) 10.

1218 [80] R. Guo, L. Lu, M. Ouyang, X. Feng, *Scientific reports*, 6 (2016) 30248.

1219 [81] K. Shinozaki, A. Suzuki, T. Tsuruta, in, *Google Patents*, 2012.

1220 [82] J.-M. Song, Y.-S. Zou, C.-C. Kuo, S.-C. Lin, *Corrosion science*, 74 (2013) 223-231.

1221 [83] M. Guo, W. Meng, X. Zhang, Z. Bai, G. Wang, Z. Wang, F. Yang, *Journal of Electronic Materials*, 48
1222 (2019) 7543-7550.

1223 [84] J. Zhu, J. Feng, Z. Guo, *RSC advances*, 4 (2014) 57671-57678.

1224 [85] Q. Li, S. Zhu, Y. Lu, *Advanced Functional Materials*, 27 (2017) 1606422.

1225 [86] H.-Y. Lee, S.-M. Lee, *Electrochemistry Communications*, 6 (2004) 465-469.

1226 [87] B. Key, R. Bhattacharyya, M. Morcrette, V. Seznec, J.-M. Tarascon, C.P. Grey, *Journal of the*
1227 *American Chemical Society*, 131 (2009) 9239-9249.

1228 [88] C. Brissot, M. Rosso, J.-N. Chazalviel, P. Baudry, S. Lascaud, *Electrochimica acta*, 43 (1998) 1569-
1229 1574.

1230 [89] Q. Yun, Y.B. He, W. Lv, Y. Zhao, B. Li, F. Kang, Q.H. Yang, *Advanced Materials*, 28 (2016) 6932-
1231 6939.

1232 [90] Y. An, H. Fei, G. Zeng, X. Xu, L. Ci, B. Xi, S. Xiong, J. Feng, Y. Qian, *Nano Energy*, 47 (2018) 503-511.

1233 [91] H. Qiu, T. Tang, M. Asif, X. Huang, Y. Hou, *Advanced Functional Materials*, 29 (2019) 1808468.

1234 [92] H. Liu, E. Wang, Q. Zhang, Y. Ren, X. Guo, L. Wang, G. Li, H. Yu, *Energy Storage Materials*, 17 (2019)
1235 253-259.
1236 [93] P. Zhu, Z. Wu, Y. Zhao, *Scripta Materialia*, 172 (2019) 119-124.
1237 [94] S.H. Wang, Y.X. Yin, T.T. Zuo, W. Dong, J.Y. Li, J.L. Shi, C.H. Zhang, N.W. Li, C.J. Li, Y.G. Guo,
1238 *Advanced Materials*, 29 (2017) 1703729.
1239 [95] C. Monroe, J. Newman, *Journal of The Electrochemical Society*, 150 (2003) A1377-A1384.
1240 [96] Y. Wang, Z. Wang, D. Lei, W. Lv, Q. Zhao, B. Ni, Y. Liu, B. Li, F. Kang, Y.-B. He, *ACS applied materials*
1241 *& interfaces*, 10 (2018) 20244-20249.
1242 [97] J.S. Wang, P. Liu, E. Sherman, M. Verbrugge, H. Tataria, *Journal of Power Sources*, 196 (2011)
1243 8714-8718.
1244 [98] Z. Du, D.L. Wood, C. Daniel, S. Kalnaus, J. Li, *Journal of Applied Electrochemistry*, 47 (2017) 405-
1245 415.
1246 [99] T. Jiang, S. Zhang, X. Qiu, W. Zhu, L. Chen, *Electrochemistry communications*, 9 (2007) 930-934.
1247 [100] D.H. Nam, R.H. Kim, D.W. Han, H.S. Kwon, *Electrochimica Acta*, 66 (2012) 126-132.
1248 [101] X.-Y. Fan, F.-S. Ke, G.-Z. Wei, L. Huang, S.-G. Sun, *Journal of Solid State Electrochemistry*, 13
1249 (2009) 1849.
1250 [102] K.-L. Lee, J.-Y. Jung, S.-W. Lee, H.-S. Moon, J.-W. Park, *Journal of power sources*, 129 (2004) 270-
1251 274.
1252 [103] C.C. Nguyen, S.-W. Song, *Electrochimica Acta*, 55 (2010) 3026-3033.
1253 [104] D. Reyter, S. Rousselot, D. Mazouzi, M. Gauthier, P. Moreau, B. Lestriez, D. Guyomard, L. Roue,
1254 *Journal of power sources*, 239 (2013) 308-314.
1255 [105] G.-b. Cho, Y.-m. Im, W.-r. Lee, S.-h. Lee, S.-y. Ji, G.-t. Kim, T.-h. Nam, K.-w. Kim, *Thin solid films*,
1256 546 (2013) 410-413.
1257 [106] G.-b. Cho, J.-k. Kim, S.-h. Lee, G.-t. Kim, J.-p. Noh, K.-k. Cho, K.-w. Kim, T.-h. Nam, H.-j. Ahn,
1258 *Electrochimica Acta*, 224 (2017) 649-659.
1259 [107] S.-W. Kang, H.-M. Xie, W. Zhang, J.-P. Zhang, Z. Ma, R.-S. Wang, X.-L. Wu, *Electrochimica Acta*,
1260 176 (2015) 604-609.
1261 [108] J. Jiang, P. Nie, B. Ding, W. Wu, Z. Chang, Y. Wu, H. Dou, X. Zhang, *ACS applied materials &*
1262 *interfaces*, 8 (2016) 30926-30932.
1263 [109] C. Zhang, W. Lv, G. Zhou, Z. Huang, Y. Zhang, R. Lyu, H. Wu, Q. Yun, F. Kang, Q.H. Yang, *Advanced*
1264 *Energy Materials*, 8 (2018) 1703404.
1265 [110] H. Ye, Z.J. Zheng, H.R. Yao, S.C. Liu, T.T. Zuo, X.W. Wu, Y.X. Yin, N.W. Li, J.J. Gu, F.F. Cao,
1266 *Angewandte Chemie*, 131 (2019) 1106-1111.
1267 [111] Z. Hou, Y. Yu, W. Wang, X. Zhao, Q. Di, Q. Chen, W. Chen, Y. Liu, Z. Quan, *ACS applied materials*
1268 *& interfaces*, 11 (2019) 8148-8154.
1269 [112] L.-L. Lu, Y. Zhang, Z. Pan, H.-B. Yao, F. Zhou, S.-H. Yu, *Energy Storage Materials*, 9 (2017) 31-38.
1270 [113] L. Qin, H. Xu, D. Wang, J. Zhu, J. Chen, W. Zhang, P. Zhang, Y. Zhang, W. Tian, Z. Sun, *ACS applied*
1271 *materials & interfaces*, 10 (2018) 27764-27770.
1272 [114] J. Luo, C.C. Fang, N.L. Wu, *Advanced Energy Materials*, 8 (2018) 1701482.
1273 [115] G.V. Zhuang, K. Xu, H. Yang, T.R. Jow, P.N. Ross, *The Journal of Physical Chemistry B*, 109 (2005)
1274 17567-17573.
1275 [116] T.K. Kim, W. Chen, C. Wang, *Journal of Power Sources*, 196 (2011) 8742-8746.
1276 [117] I. Geoffroy, P. Willmann, K. Mesfar, B. Carre, D. Lemordant, *Electrochimica acta*, 45 (2000) 2019-
1277 2027.
1278 [118] T. Liu, L. Zhao, D. Wang, J. Zhu, B. Wang, C. Guo, *RSC advances*, 3 (2013) 25648-25651.
1279 [119] G.M. Veith, N.J. Dudney, *Journal of The Electrochemical Society*, 158 (2011) A658.
1280 [120] S. Ohara, J. Suzuki, K. Sekine, T. Takamura, *Journal of power sources*, 119 (2003) 591-596.
1281 [121] S. Ohara, J. Suzuki, K. Sekine, T. Takamura, *Journal of power sources*, 136 (2004) 303-306.
1282 [122] J. Liu, Y. Li, X. Huang, R. Ding, Y. Hu, J. Jiang, L. Liao, *Journal of Materials Chemistry*, 19 (2009)
1283 1859-1864.

- 1284 [123] X. Xiao, P. Liu, J.S. Wang, M. Verbrugge, M.P. Balogh, *Electrochemistry Communications*, 13
1285 (2011) 209-212.
- 1286 [124] C. Wang, Y. Li, Y.-S. Chui, Q.-H. Wu, X. Chen, W. Zhang, *Nanoscale*, 5 (2013) 10599-10604.
- 1287 [125] W. Mei, J. Huang, L. Zhu, Z. Ye, Y. Mai, J. Tu, *Journal of Materials Chemistry*, 22 (2012) 9315-
1288 9321.
- 1289 [126] B. Varghese, M. Reddy, Z. Yanwu, C.S. Lit, T.C. Hoong, G. Subba Rao, B. Chowdari, A.T.S. Wee,
1290 C.T. Lim, C.-H. Sow, *Chemistry of Materials*, 20 (2008) 3360-3367.
- 1291 [127] C.-H. Lai, K.-W. Huang, J.-H. Cheng, C.-Y. Lee, W.-F. Lee, C.-T. Huang, B.-J. Hwang, L.-J. Chen,
1292 *Journal of Materials Chemistry*, 19 (2009) 7277-7283.
- 1293 [128] in, 2013.
- 1294 [129] M.S. Jo, S. Ghosh, S.M. Jeong, Y.C. Kang, J.S. Cho, *Nano-Micro Letters*, 11 (2019) 3.
- 1295 [130] W. Zhou, J.-L. Zheng, Y.-H. Yue, L. Guo, *Nano Energy*, 11 (2015) 428-435.
- 1296 [131] P. Nithyadharseni, M. Reddy, B. Nalini, B. Chowdari, *Materials Letters*, 150 (2015) 24-27.
- 1297 [132] E. Hosono, S. Fujihara, I. Honma, H. Zhou, *Electrochemistry communications*, 8 (2006) 284-288.
- 1298 [133] Q. Sa, Y. Wang, *Journal of Power Sources*, 208 (2012) 46-51.
- 1299 [134] S. Ni, T. Li, X. Lv, X. Yang, L. Zhang, *Electrochimica Acta*, 91 (2013) 267-274.
- 1300 [135] Y. Fu, Z. Yang, X. Li, X. Wang, D. Liu, D. Hu, L. Qiao, D. He, *Journal of Materials Chemistry A*, 1
1301 (2013) 10002-10007.
- 1302 [136] X. Li, A. Dhanabalan, K. Bechtold, C. Wang, *Electrochemistry Communications*, 12 (2010) 1222-
1303 1225.
- 1304 [137] W. Yang, G. Cheng, C. Dong, Q. Bai, X. Chen, Z. Peng, Z. Zhang, *Journal of Materials Chemistry A*,
1305 2 (2014) 20022-20029.
- 1306 [138] S. Ni, X. Yang, T. Li, *Journal of Materials Chemistry*, 22 (2012) 2395-2397.
- 1307 [139] S. Ni, X. Yang, T. Li, *Materials Chemistry and Physics*, 132 (2012) 1103-1107.
- 1308 [140] X. Wang, L. Sun, X. Hu, R.A. Susantyoko, Q. Zhang, *Journal of Power Sources*, 280 (2015) 393-
1309 396.
- 1310 [141] H. Liu, L. Hu, Y.S. Meng, Q. Li, *Nanoscale*, 5 (2013) 10376-10383.
- 1311 [142] B. Qu, L. Hu, Q. Li, Y. Wang, L. Chen, T. Wang, *ACS applied materials & interfaces*, 6 (2014) 731-
1312 736.
- 1313 [143] J. Yuan, C. Chen, Y. Hao, X. Zhang, S. Gao, R. Agrawal, C. Wang, Z. Xiong, H. Yu, Y. Xie, *Journal of*
1314 *Electroanalytical Chemistry*, 787 (2017) 158-162.
- 1315 [144] H. Long, T. Shi, S. Jiang, S. Xi, R. Chen, S. Liu, G. Liao, Z. Tang, *Journal of Materials Chemistry A*, 2
1316 (2014) 3741-3748.
- 1317 [145] Q. Li, X. Miao, C. Wang, L. Yin, *Journal of Materials Chemistry A*, 3 (2015) 21328-21336.
- 1318 [146] T. Takamura, S. Ohara, M. Uehara, J. Suzuki, K. Sekine, *Journal of Power Sources*, 129 (2004) 96-
1319 100.
- 1320 [147] M. Uehara, J. Suzuki, K. Tamura, K. Sekine, T. Takamura, *Journal of power sources*, 146 (2005)
1321 441-444.
- 1322 [148] T. Takamura, M. Uehara, J. Suzuki, K. Sekine, K. Tamura, *Journal of power sources*, 158 (2006)
1323 1401-1404.
- 1324 [149] S. Wang, L. Niu, C. Chen, Y. Pang, B. Liao, Z. Zhong, P. Lu, P. Li, X. Wu, J.W. Coenen, *Materials*
1325 *Science and Engineering: A*, 730 (2018) 244-261.
- 1326 [150] J. Jiang, J. Liu, R. Ding, X. Ji, Y. Hu, X. Li, A. Hu, F. Wu, Z. Zhu, X. Huang, *The Journal of Physical*
1327 *Chemistry C*, 114 (2010) 929-932.
- 1328 [151] Y. Li, B. Tan, Y. Wu, *Nano letters*, 8 (2008) 265-270.
- 1329 [152] Y. Wang, H. Xia, L. Lu, J. Lin, *ACS nano*, 4 (2010) 1425-1432.
- 1330 [153] L. Zhan, S. Wang, L.-X. Ding, Z. Li, H. Wang, *Electrochimica Acta*, 135 (2014) 35-41.
- 1331 [154] H. Wu, M. Xu, Y. Wang, G. Zheng, *Nano Research*, 6 (2013) 167-173.
- 1332 [155] S. Chen, M. Wang, J. Ye, J. Cai, Y. Ma, H. Zhou, L. Qi, *Nano Research*, 6 (2013) 243-252.
- 1333 [156] L. Zhang, H.B. Wu, X.D.W. Lou, *Materials Horizons*, 1 (2014) 133-138.
- 1334 [157] D. Cai, D. Li, L.-X. Ding, S. Wang, H. Wang, *Electrochimica Acta*, 192 (2016) 407-413.

1335 [158] S. Dong, H. Wang, L. Gu, X. Zhou, Z. Liu, P. Han, Y. Wang, X. Chen, G. Cui, L. Chen, *Thin Solid Films*,
1336 519 (2011) 5978-5982.

1337 [159] Y. Tang, L. Hong, Q. Wu, J. Li, G. Hou, H. Cao, L. Wu, G. Zheng, *Electrochimica Acta*, 195 (2016)
1338 27-33.

1339 [160] S. Chen, Y. Xin, Y. Zhou, Y. Ma, H. Zhou, L. Qi, *Energy & Environmental Science*, 7 (2014) 1924-
1340 1930.

1341 [161] X. Wang, B. Liu, X. Hou, Q. Wang, W. Li, D. Chen, G. Shen, *Nano Research*, 7 (2014) 1073-1082.

1342 [162] L. Tian, A. Yuan, *Journal of Power Sources*, 192 (2009) 693-697.

1343 [163] Z.-J. Zhang, Q.-Y. Zeng, S.-L. Chou, X.-J. Li, H.-J. Li, K. Ozawa, H.-K. Liu, J.-Z. Wang, *Electrochimica*
1344 *Acta*, 133 (2014) 570-577.

1345 [164] M.-S. Balogun, Y. Zhu, W. Qiu, Y. Luo, Y. Huang, C. Liang, X. Lu, Y. Tong, *ACS applied materials &*
1346 *interfaces*, 7 (2015) 25991-26003.

1347 [165] Y. Liu, R. Xiao, Y. Fang, P. Zhang, *Electrochimica Acta*, 211 (2016) 1041-1047.

1348 [166] Z. Bi, M.P. Paranthaman, P.A. Menchhofer, R.R. Dehoff, C.A. Bridges, M. Chi, B. Guo, X.-G. Sun,
1349 S. Dai, *Journal of Power Sources*, 222 (2013) 461-466.

1350 [167] H. Choi, H. Park, J.H. Um, W.-S. Yoon, H. Choe, *Applied Surface Science*, 411 (2017) 363-367.

1351 [168] G. Lorang, M.D.C. Belo, A. Simoes, M. Ferreira, *Journal of The Electrochemical Society*, 141 (1994)
1352 3347-3356.

1353 [169] J.P. Maranchi, A.F. Hepp, P.N. Kumta, *Materials Science and Engineering: B*, 116 (2005) 327-340.

1354 [170] Y. Wen, L. Shao, P. Zhao, B. Wang, G. Cao, Y. Yang, *Journal of Materials Chemistry A*, 5 (2017)
1355 15752-15758.

1356 [171] W. Fredriksson, K. Edström, *Electrochimica acta*, 79 (2012) 82-94.

1357 [172] G. Zhang, K. Takashima, Y. Higo, *Materials Science and Engineering: A*, 426 (2006) 95-100.

1358 [173] X. Li, L. Qiao, D. Li, X. Wang, W. Xie, D. He, *Journal of Materials Chemistry A*, 1 (2013) 6400-6406.

1359 [174] D.H. Sim, X. Rui, J. Chen, H. Tan, T.M. Lim, R. Yazami, H.H. Hng, Q. Yan, *RSC advances*, 2 (2012)
1360 3630-3633.

1361 [175] C. Jacob, T. Lynch, A. Chen, J. Jian, H. Wang, *Journal of power sources*, 241 (2013) 410-414.

1362 [176] L. Xue, S.V. Savilov, V.V. Lunin, H. Xia, *Advanced Functional Materials*, 28 (2018) 1705836.

1363 [177] S. Shironita, N. Ihsan, K. Konakawa, K. Souma, M. Umeda, *Electrochimica Acta*, 295 (2019) 1052-
1364 1056.

1365 [178] M. Park, G. Wang, H.-K. Liu, S. Dou, *Electrochimica acta*, 51 (2006) 5246-5249.

1366 [179] K. Peng, J. Jie, W. Zhang, S.-T. Lee, *Applied Physics Letters*, 93 (2008) 033105.

1367 [180] L. Hu, H. Wu, S.S. Hong, L. Cui, J.R. McDonough, S. Bohy, Y. Cui, *Chemical Communications*, 47
1368 (2011) 367-369.

1369 [181] J.-H. Cho, X. Li, S.T. Picraux, *Journal of Power Sources*, 205 (2012) 467-473.

1370 [182] V. Aravindan, K. Jinesh, R.R. Prabhakar, V.S. Kale, S. Madhavi, *Nano Energy*, 2 (2013) 720-725.

1371 [183] W. Zeng, F. Zheng, R. Li, Y. Zhan, Y. Li, J. Liu, *Nanoscale*, 4 (2012) 2760-2765.

1372 [184] Y.-Q. Chu, Z.-W. Fu, Q.-Z. Qin, *Electrochimica Acta*, 49 (2004) 4915-4921.

1373 [185] H. Yue, F. Li, Z. Yang, J. Tang, X. Li, D. He, *Materials Letters*, 120 (2014) 39-42.

1374 [186] X. Xu, J. Liu, R. Hu, J. Liu, L. Ouyang, M. Zhu, *Chemistry—A European Journal*, 23 (2017) 5198-
1375 5204.

1376 [187] G.-P. Kim, S. Park, I. Nam, J. Park, J. Yi, *Journal of power sources*, 237 (2013) 172-177.

1377 [188] G.-P. Kim, I. Nam, N.D. Kim, J. Park, S. Park, J. Yi, *Electrochemistry communications*, 22 (2012)
1378 93-96.

1379 [189] H.-C. Liu, S.-K. Yen, *Journal of Power Sources*, 166 (2007) 478-484.

1380 [190] M. Laurenti, N. Garino, S. Porro, M. Fontana, C. Gerbaldi, *Journal of Alloys and Compounds*, 640
1381 (2015) 321-326.

1382 [191] V. Channu, R. Bobba, R. Holze, *Colloids and Surfaces A: Physicochemical and Engineering*
1383 *Aspects*, 436 (2013) 245-251.

1384 [192] K. Feng, H.W. Park, X. Wang, D.U. Lee, Z. Chen, *Electrochimica Acta*, 139 (2014) 145-151.

1385 [193] Q. Chu, B. Yang, W. Wang, W. Tong, X. Wang, X. Liu, J. Chen, *ChemistrySelect*, 1 (2016) 5569-
1386 5573.

1387 [194] H.-Y. Cheng, P.-Y. Cheng, X.-F. Chuah, C.-L. Huang, C.-T. Hsieh, J. Yu, C.-H. Lin, S.-Y. Lu, *Chemical*
1388 *Engineering Journal*, 374 (2019) 201-210.

1389 [195] E. Pomerantseva, K. Gerasopoulos, X. Chen, G. Rubloff, R. Ghodssi, *Journal of Power Sources*,
1390 206 (2012) 282-287.

1391 [196] X. Li, D. Li, Z. Wei, X. Shang, D. He, *Electrochimica Acta*, 121 (2014) 415-420.

1392 [197] S.K. Martha, N.J. Dudney, J.O. Kiggans, J. Nanda, *Journal of The Electrochemical Society*, 159
1393 (2012) A1652.

1394 [198] S. Flandrois, B. Simon, *Carbon*, 37 (1999) 165-180.

1395 [199] F. Barbir, *PEM Fuel Cells: Theory and Practice*, (2005) 73-113.

1396 [200] J.W. Choi, L. Hu, L. Cui, J.R. McDonough, Y. Cui, *Journal of Power Sources*, 195 (2010) 8311-8316.

1397 [201] J. Guo, A. Sun, C. Wang, *Electrochemistry communications*, 12 (2010) 981-984.

1398 [202] M. Shafiei, A.T. Alpas, *Journal of Power Sources*, 196 (2011) 7771-7778.

1399 [203] Y. Shi, B. Wang, *Progress in Natural Science: Materials International*, 24 (2014) 56-60.

1400 [204] G. Zhou, F. Li, H.-M. Cheng, *Energy & Environmental Science*, 7 (2014) 1307-1338.

1401 [205] H. Lu, J. Hagberg, G. Lindbergh, A. Cornell, *Nano Energy*, 39 (2017) 140-150.

1402 [206] H. Lu, J. Hagberg, G. Lindbergh, A. Cornell, *Batteries*, 4 (2018) 17.

1403 [207] R.A. Susantyoko, X. Wang, Q. Xiao, E. Fitzgerald, Q. Zhang, *Carbon*, 68 (2014) 619-627.

1404 [208] C.-H. Hsu, H.-H. Lin, Y.-H. Liu, H.-P. Lin, *New Journal of Chemistry*, 42 (2018) 9058-9064.

1405 [209] H. Wolf, Z. Pajkic, T. Gerdes, M. Willert-Porada, *Journal of Power Sources*, 190 (2009) 157-161.

1406 [210] L.-L. Zhang, Z. Li, X.-L. Yang, X.-K. Ding, Y.-X. Zhou, H.-B. Sun, H.-C. Tao, L.-Y. Xiong, Y.-H. Huang,
1407 *Nano Energy*, 34 (2017) 111-119.

1408 [211] S. Chu, Y. Zhong, R. Cai, Z. Zhang, S. Wei, Z. Shao, *Small*, 12 (2016) 6724-6734.

1409 [212] Z. Liu, S. Bai, B. Liu, P. Guo, M. Lv, D. Liu, D. He, *Journal of Materials Chemistry A*, 5 (2017) 13168-
1410 13175.

1411 [213] J. Guo, X. Chen, C. Wang, *Journal of Materials Chemistry*, 20 (2010) 5035-5040.

1412 [214] K. Fu, O. Yildiz, H. Bhanushali, Y. Wang, K. Stano, L. Xue, X. Zhang, P.D. Bradford, *Advanced*
1413 *Materials*, 25 (2013) 5109-5114.

1414 [215] J.W. Hu, Z.P. Wu, S.W. Zhong, W.B. Zhang, S. Suresh, A. Mehta, N. Koratkar, *Carbon*, 87 (2015)
1415 292-298.

1416 [216] A.M. Gaikwad, B.V. Khau, G. Davies, B. Hertzberg, D.A. Steingart, A.C. Arias, *Advanced Energy*
1417 *Materials*, 5 (2015) 1401389.

1418 [217] L. Hu, F. La Mantia, H. Wu, X. Xie, J. McDonough, M. Pasta, Y. Cui, *Advanced Energy Materials*, 1
1419 (2011) 1012-1017.

1420 [218] S.-J. Kim, M.-C. Kim, S.-B. Han, G.-H. Lee, H.-S. Choe, S.-H. Moon, D.-H. Kwak, S. Hong, K.-W. Park,
1421 *Journal of Industrial and Engineering Chemistry*, 49 (2017) 105-111.

1422 [219] K. Lin, X. Qin, M. Liu, X. Xu, G. Liang, J. Wu, F. Kang, G. Chen, B. Li, *Advanced Functional Materials*,
1423 29 (2019) 1903229.

1424 [220] D. Chao, X. Xia, J. Liu, Z. Fan, C.F. Ng, J. Lin, H. Zhang, Z.X. Shen, H.J. Fan, *Advanced materials*, 26
1425 (2014) 5794-5800.

1426 [221] R. Mo, D. Rooney, K. Sun, H.Y. Yang, *Nature communications*, 8 (2017) 1-9.

1427 [222] J. He, Q. Li, Y. Chen, C. Xu, K. Zhou, X. Wang, W. Zhang, Y. Li, *Carbon*, 114 (2017) 111-116.

1428 [223] Y. Tang, J. Sha, N. Wang, R. Zhang, L. Ma, C. Shi, E. Liu, N. Zhao, *Carbon*, 158 (2020) 536-544.

1429 [224] M.A. Peña-Guerrero, C. Leitherer, S. de Mink, A. Wofford, L. Kewley, *The Astrophysical Journal*,
1430 847 (2017) 107.

1431 [225] M. Henckens, P. Driessen, E. Worrell, *Resources, Conservation and recycling*, 93 (2014) 1-8.

1432 [226] T. Or, S.W. Gourley, K. Kaliyappan, A. Yu, Z. Chen, *Carbon Energy*, (2020).

1433 [227] J. Marshall, D. Gastol, R. Sommerville, B. Middleton, V. Goodship, E. Kendrick, *Metals*, 10 (2020)
1434 773.

1435 [228] H. Wang, J. Liu, X. Bai, S. Wang, D. Yang, Y. Fu, Y. He, *Waste Management*, 91 (2019) 89-98.

- 1436 [229] A. Savvatimskiy, Carbon, 43 (2005) 1115-1142.
- 1437 [230] G.-F. Yang, S.-K. Joo, Electrochimica Acta, 170 (2015) 263-268.
- 1438 [231] D.J. Noelle, M. Wang, Y. Qiao, Journal of Power Sources, 399 (2018) 125-132.
- 1439 [232] S. Poetz, B. Fuchsbichler, M. Schmuck, S. Koller, Journal of applied electrochemistry, 44 (2014)
- 1440 989-994.
- 1441